ELECTRON SPIN RESONANCE AND OPTICAL STUDIES OF DOPED COPPER (II) TETRAHEDRAL COMPLEXES

BY

Simon Paul Cashion B. Sc. (Tas.)

A thesis submitted in partial fulfilment
of the requirements for the degree of
Bachelor of Science with Honours in the
University of Tasmania .

DEPARTMENT OF CHEMISTRY
UNIVERSITY OF TASMANIA

November , 1989

To the best of my knowledge and belief, this thesis contains no copy or paraphrase of material previously published or written by another person, except where due reference is made in the text.

Simon Cashion

November 1989

CONTENTS

ACKNOWLEDGEMENT

Dr. M. A. Hitchman has been a constant source of advice, encouragement, and understanding throughout this project, and for this I wish to express my sincere thanks. I also thank Dr. Horst Stratemeier for his companionship and tireless assistance with the PRIME computer programs. A special thanks must also go to my mentor, Dr. P. W. Smith, for his continual interest in my well-being during my entire academic career at this University. His persistence in keeping me on the path of righteousness when all seemed lost deserves commendation. Thanks also to my typist Sandra Petrie and to Mr. C. Narckowicz for assistance with the E.S.R. spectrometer. Finally, I wish to thank the " class of '89 " for making this year rewarding, enjoyable and one that will certainly not be forgotten.

ABSTRACT

This report presents an investigation of a pseudotetrahedral bromocuprate (II) compound. The bromocuprates exhibit a great structural diversity, however, the comparatively rare compressed tetrahedral compounds have been somewhat neglected. The determination of the electronic and geometric structure of these compounds has implications in the analysis of active sites in copper blue proteins.

Electron Spin Resonance (E.S.R.) and optical spectra have been measured at low temperature, for single crystals of copper (II) doped into bis-(ethylenediammoniummonobromide) tetrabromozincate (II), $(enH.HBr)_2ZnBr_4$. The room temperature powder reflectance spectrum has also been measured for this compound, along with that of the pure zinc analogue.

The transition energies derived from the electronic spectra have been assigned and compared to the respective transitions based on previous studies. With the aid of a computer program, a set of theoretical transition energies has been calculated utilizing the Angular Overlap Model. Adjusting these to fit the observed values confirms the presence of a distorted tetrahedral geometry for the guest ion.

At 77K, the E.S.R. spectrum of $(enH_2)_2Zn[Cu]Br_6$ exhibits well resolved copper hyperfine and bromine superhyperfine couplings. Computer simulation techniques have produced optimum values for these parameters, which suggest that the principal z-axis of the superhyperfine tensor does not coincide with the copper-bromine bond direction. The bonding in the guest $[CuBr_4]^{2-}$ ion has been described in terms of the relative unpaired electron density within the bromine 4s and 4p orbitals, which shows an increased covalency when compared with the chlorine counterpart. A highly rhombic **g** tensor results in an unusual groundstate. The calculated mixing coefficients and corresponding wavefunction parameters show that the $d_{Z}2$ orbital makes a small but significant contribution by mixing with the pure $d_{X}2\text{-}_{Y}2$ orbital.

CHAPTER 1.
INTRODUCTION

Tetrahedral coordination of the copper (II) ion is less common than octahedral coordination, with the square planar geometry being favoured in four-coordinated Cu (II) complexes[1]. *Pseudo*tetrahedral copper (II) complexes, in which a regular tetrahedral geometry of T_d symmetry is distorted by a compression along the z axis, are far less numerous than either the square-planar or the distorted octahedral analogues . However, these compounds are attracting attention, since distorted tetrahedral copper (II) chromophores are known to be present in some metalloenzymes and metalloproteins[2].

The Jahn-Teller theorem[3] predicts that the degenerate ground state of a tetrahedral d^9 ion such as $[CuBr_4]^{2-}$ will be electronically unstable. Distortion of the complex results in a ' flattened ' tetrahedral structure with a Br - Cu - Br angle (denoted α) for opposing bromine ligands of ~123^o . The distorted structure adopted results from a balance of ligand-ligand repulsions favouring the T_d symmetry, and ligand field stabilisation favouring D_{4h} symmetry.[4] Hence, one predominantly deals with pseudotetrahedral complexes which are *variously* distorted. The most frequent types observed consist of tetragonal (D_{2d}) and rhombic (C_{2v}) distortions[1] [Figure 1.1].

Regardless of which of the above factors is dominant, the observed flattening must be elucidated in terms of the electronic structure of the $[CuBr_4]^{2-}$ ion. Two investigative techniques, sensitive to the electronic environment of the metal ion in question, are Electron Spin Resonance (E.S.R) spectroscopy and Electronic (or Optical) spectroscopy. Both utilize the fact that a d^9 configuration[5] of copper results in an unpaired electron and an incomplete d shell. When used in combination, these techniques are a powerful tool, as they deal with the groundstate and excited states respectively.

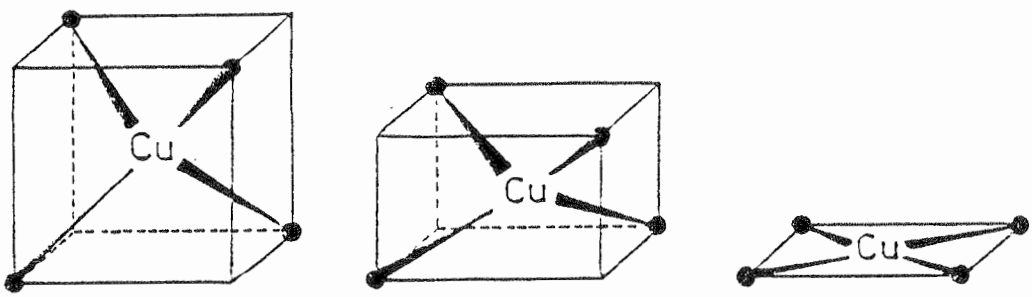

(a) (b) (c)

Figure 1.1 : Geometries of the $[CuBr_4]^{2-}$ ion

a) regular tetrahedron (T_d)

b) flattened tetrahedron (D_{2d})

c) square planar (D_{4h})

The most informative results are obtainable when the $[CuBr_4]^{2-}$ ion is ' isolated ' from external influences. This effect can be achieved by doping a small amount of the copper (II) ion into a diamagnetic host lattice. In many earlier studies of this nature, (see, for example, ref. 6) this host lattice was considered as merely providing a matrix to hold the copper (II) ion in a fixed orientation in space. The guest was subsequently assumed to adopt a geometry similar to that of the pure copper (II) compounds. It has since been recognized[7] that in these doping experiments, the host lattice may induce distortions upon the guest complex, and these may provide information on the balance between the electronic and steric forces that decide the equilibrium nuclear geometry of the copper compound.

This work presents a study of the E.S.R and electronic spectra of Cu^{2+} doped into various zinc (II) bromo complexes, and parallels a previous investigation[8] concerned with zinc (II) chloro complexes as hosts. For one of the

copper (II) complexes, the electronic structure and probable geometry of the guest $[CuBr_4]^{2-}$ ion has been deduced and quantified. In addition, a significant hyperfine and superhyperfine coupling was observed in the E.S.R spectrum for this compound, allowing an analysis of the unpaired electron spin density in the complex.

1.1 Previous Studies

The chlorocuprates exhibit a wide range of stereochemistries , and have frequently been used to test theoretical models of the bonding in metal complexes[9]. The bromocuprates, however, have not been subjected to such a multitude of investigations.

Willett et al.[10] measured the E.S.R spectra of copper-doped potassium tetrabromopalladate, with both hyperfine and superhyperfine structures being resolved at room temperature. In this case, however, the $[CuBr_4]^{2-}$ ion adopted a square-planar geometry. This is a less complicated situation than for distorted tetrahedra, as the four ligands are equivalent. In this work, the marked difference between angles α and β results in *two pairs* of equivalent ligands. In addition, for a square-planar structure, the z - axis of the superhyperfine tensor for each bromine is required by symmetry to lie along the metal-ligand bond direction. It is known that this does not hold for pseudotetrahedral geometries.

D. K. De[11] performed E.S.R and optical measurements on tetramethyl-ammonium tetrabromocuprate (II) $(Me_4N)_2CuBr_4$. The resonance signal produced in X-, K-, and Q-band E.S.R spectra was too broad to be analysed, as is the case for many pure copper compounds. Thus no hyperfine or superhyperfine couplings could be resolved, and only g values were reported. These values are somewhat tenuous, due to the lack of a detailed X-ray structure for $(Me_4N)_2CuBr_4$ at the time of publication. In the optical study, three d-d transitions were observed, and assigned on the basis of a D_{2d} symmetry with a $^2B_2$ groundstate.

Numerous studies have been devoted to the investigation of the structure and bonding of bromocuprate derivatives coordinated to bulky organic ligands. These include reports on $CuBr_2(L)$, where L = 1-methylpyrimidine-2-thione[12], 6-nitro-2,3-di-(2-pyridyl)-quinoxaline[13], and PhCOpy[14]. All compounds have been determined to contain distorted tetrahedral $[CuBr_4]^{2-}$ units through the use of optical and E.S.R measurements. However, the nature of these studies precludes any detailed discussion of aspects relevant to the present work.

The lack of thorough documentation concerning the electronic and geometric structure of pseudotetrahedral copper (II) bromide complexes has prompted the present study.

CHAPTER 2.
COMPOUNDS STUDIED

2.1 Introduction

For the complexes investigated in this report, no novel preparative methods were employed. The general technique used for chlorocuprates, as described by Deeth[15], was extended to incorporate the bromocuprates.

2.2 Pure Compounds

Samples of ethylenediammonium tetrabromocuprate (II) $(enH_2)CuBr_4$ and bis-(ethylenediammonium) hexabromozincate (II) $(enH_2)_2ZnBr_6$ were available, having been prepared by M. Riley, University of Tasmania.

In this work, crystals of ethylenediammonium tetrabromozincate (II) $(enH_2)ZnBr_4$, tetramethylammonium tetrabromozincate (II) $(Me_4N)_2ZnBr_4$, tetraethylammonium tetrabromozincate (II) $(Et_4N)_2ZnBr_4$ and dicesium tetrabromocuprate Cs_2CuBr_4 were all prepared by slow evaporation of dilute HBr solutions containing stoichiometric quantities of ethylenediammonium dibromide $(enH_2)Br_2$ and the appropriate metal bromide. Attempts to prepare bis-(ethylenediammonium) hexabromocuprate (II) $(enH_2)_2CuBr_6$ using the method described by Anderson and Willett[16] proved unsuccessful. Long prismatic needles were produced from the evaporation of an HBr solution of $CuBr_2$ with a large excess (i.e > 2:1) of $(enH_2)Br_2$. Many of the needles appeared transparent, instead of the dark red colour that was expected. The recrystallization of excess $(enH_2)Br_2$ was believed to be the cause of this. Powder reflectance spectra later confirmed that the compound made was not $(enH_2)_2CuBr_6$.

2.3 Doped Systems

Samples of the copper doped systems trirubidium pentabromozincate (II) $Rb_3Zn[Cu]Br_5$, tetraethylammonium tetrabromozincate (II) $(Et_4N)_2Zn[Cu]Br_4$, tetramethylammonium tetrabromozincate (II) $(Me_4N)_2Zn[Cu]Br_4$, dicesium tetrabromozincate (II) $Cs_2Zn[Cu]Br_4$, and ethylenediammonium hexabromozincate (II) $(enH_2)_2Zn[Cu]Br_6$ were prepared by adding approximately 0.1% w/w of $CuBr_2$ to a dilute HBr solution of the pure analogue. Many of these crystals exhibited defects such as twinning, and thus were unsuitable for the experimental techniques pertinent to this work. However, some homogeneous crystals were grown, and subsequently used for investigation.

2.4 Crystal Structures of Host Zinc Compounds

For the compounds of known crystal structure, Table 2.1 displays the relevant crystal parameters.

The crystal structure of $(enH_2)_2ZnBr_6$ has been solved, but details are, as yet, unpublished (Dr. M. A. Hitchman, University of Tasmania). The structure of Cs_2ZnBr_4 has been determined[17] and refined[18], and found to be isomorphous to Cs_2ZnCl_4. Similarly, crystal structure refinements for Rb_3ZnBr_5 have also been cited[18]. For $(Me_4N)_2ZnBr_4$, the crystal structure is reported both at room temperature[19] and in its low temperature phase[19]. According to Trouelan, upon cooling from room temperature to 193K, a phase change in $(Me_4N)_2ZnBr_4$ occurs. It transforms from an orthorhombic system with space group *Pnma* to a monoclinic arrangement with space group $P2_1/a$. In this work, the importance of crystal orientation and symmetry implies that such information must not be overlooked. The structure of $(enH_2)_2CuBr_6$[16] is also relevant, and is cited later.

It should be noted that, in the context of this work, the term isomorphous does not necessarily imply that two structures are identical. Although compounds may be reported as being isomorphous, geometries of the complex anions are often dissimilar, which has a marked effect on the information important to this project.

Table 2.1 Crystallographic Data for the Zinc Host Compounds

	$(enH_2)_2ZnBr_6$	Cs_2ZnBr_4	$(Me_4N)_2ZnBr_4$ *	Rb_3ZnBr_5
space group	Pnma	Pnma	$P2_1/a$	Pnma
a	6.719	10.202	12.534	9.679
b	19.923	7.738	9.142	10.496
c	6.4341	3.539	15.772	13.443
Zn - Br1	2.3964	2.396	2.404	2.384
Zn - Br2	2.3964	2.401	2.414	2.416
Zn - Br3	2.4099	2.394	2.339	2.390
Zn - Br4	2.4558	2.394	2.400	2.390
Br1-Zn-Br2	123.30	115.5	110.0	109.4
Br1-Zn-Br3	108.39	109.7	119.5	110.2
Br1-Zn-Br4	104.04	109.4	107.5	110.2
Br3-Zn-Br4	107.66	109.0	109.2	115.7

All bondlengths quoted are in Angstroms (Å)

All bond angles quoted are in degrees

* data corresponding to low temperature phase

2.4 Crystal Morphology

The measurement of single crystal spectra is important as the building of complex ions into a crystal causes the orientations and geometries of the molecules to be fixed, so that the polarization vector of the incident light can be defined with respect to the molecular axes.[20] In order to obtain meaningful results from single

crystal studies, it is therefore necessary to determine the *extinction directions* of the crystal under observation. This is the position in which the electric vector of the light will pass from the polariser, through the crystal, with no change in the plane of polarisation. In orthorhombic systems, the three extinction directions are mutually perpendicular, corresponding to the alignment of the polarisation plane along the crystal axes[21]. For a monoclinic crystal, such as that for $(enH_2)_2ZnBr_6$, one extinction direction lies along the b crystal axis. The other two, however, may lie anywhere in the (010) or ac plane, as the a and c axes are no longer orthogonal. The orientation of the crystal axes in $(enH_2)_2ZnBr_6$ is depicted in Figure 2.2, together with the configuration of the complex anion in the unit cell.

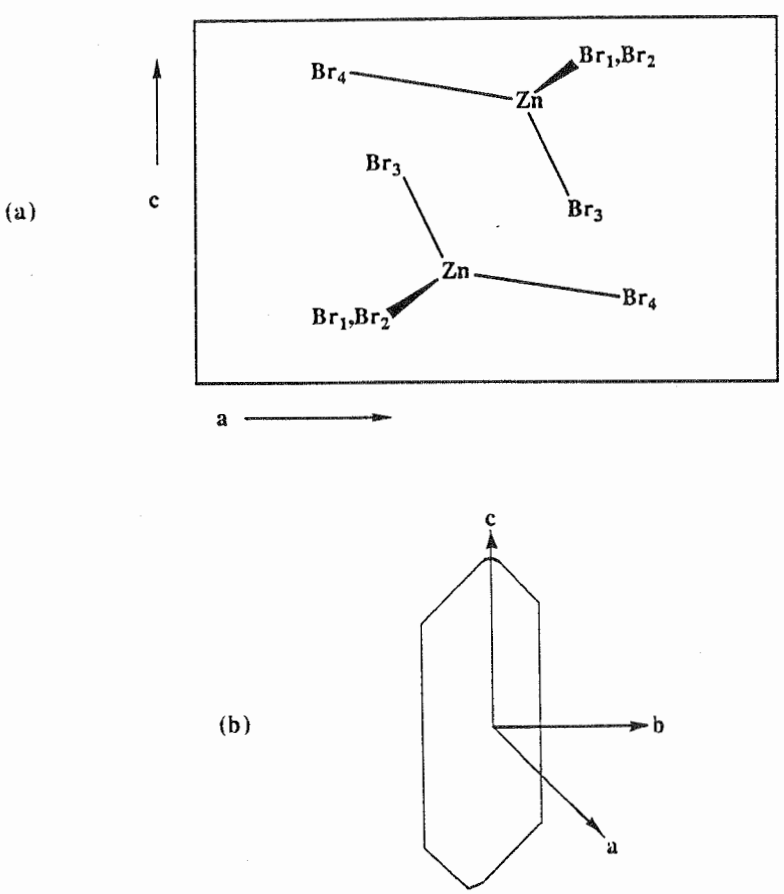

Figure 2.2 : a) configuration of $[ZnBr_4]^{2-}$ ion in the unit cell

b) orientation of crystal axes for $(enH_2)_2ZnBr_6$

CHAPTER 3.
ELECTRONIC SPECTROSCOPY

3.1 Theoretical Outline

In general, electronic spectra allow the measurement of the energies of the component states in a molecule. The geometry of the complex[22] and the transition type are the dominant factors governing the energy and intensity of the observed transition. In this work, the two types of transition of principal interest are the ' d-d ' and charge transfer (CT) transitions.

The former group correspond to electric dipole transitions between states of equal parity, and are thus formally Laporte forbidden[5]. However, due to the presence of spin-orbit and vibronic coupling, electronically forbidden spectra may become weakly vibronically allowed[23]. This gives rise to absorptions with molar extinction coefficients (ε) in the range 1 - 1000 cm^{-1} $mole^{-1}$. For the charge-transfer transitions, some of which may now be Laporte allowed, more intense absorptions occur (i.e $\varepsilon \sim 10^3$ - 10^6 cm^{-1} $mole^{-1}$) these being typically at higher energy.

Both types of transitions may exhibit intensity changes as a function of the orientation of the electric vector. These changes, known as polarisations, are extremely important, as predictions determined from group theory may be used in assigning the observed transitions to a unique set of energy levels.

3.2 Experimental

All optical spectra were recorded on a ' CARY 17 ' spectrophotometer, over the range 4000 cm^{-1} to 25000 cm^{-1}. For low temperature measurements, a ' Cryodyne Model 2A ' closed-cycle cryostat was used, permitting temperatures of between 10 and 17K to be attained.

The doped systems were investigated using single crystal spectra. A

small ' viewing hole ' was cut into a square of copper foil and the crystal was secured over this with a small spot of silicone vacuum grease. The incident light was polarised with a ' Glan -Thompson ' polarising prism, and the crystal was mounted so that an extinction direction was parallel to the plane of polarisation of the light. For each crystal, spectra were recorded for two orthogonal orientations of the plane of polarisation.

Single crystal studies were impossible for the *pure* copper (II) complexes, as the light absorption was too intense. Pure compounds were therefore measured as a mull, consisting of a finely ground crystal combined with silicone vacuum grease. The resulting paste was smeared onto a small glass slide and placed on the mount in a similar fashion to the copper foil. It should be noted that with studies of this nature, orientation has no relevance for the results.

3.3 Polarised Electronic Spectra

Single crystal polarised electronic spectra were measured for the doped systems of $(Me_4N)_2Zn[Cu]Br_4$ and $(enH_2)_2Zn[Cu]Br_6$. By analogy with the E.S.R data, measurements for the latter compound involve the bc plane. Spectra corresponding to the plane of polarisation being alligned along the b and c crystal axes were recorded, both at room temperature and at approximately 12K. Results for the low temperature spectra are presented in Figures 3.1(a) and (b).

3.4 Powder Reflectance Spectra

In the region below 5300 cm^{-1}, the single crystal spectra become complicated due to the presence of infra-red overtones and/or combination bands of the counter cation. To investigate the possibility of transitions in this area, the powder reflectance spectrum of $(enH_2)_2Zn[Cu]Br_6$ was recorded on a 'Beckman' DK2A spectrophotometer. As a reference, similar measurements were made on the pure zinc host lattice $(enH_2)_2ZnBr_6$. Both spectra are displayed in Figures 3.1(c) and (d).

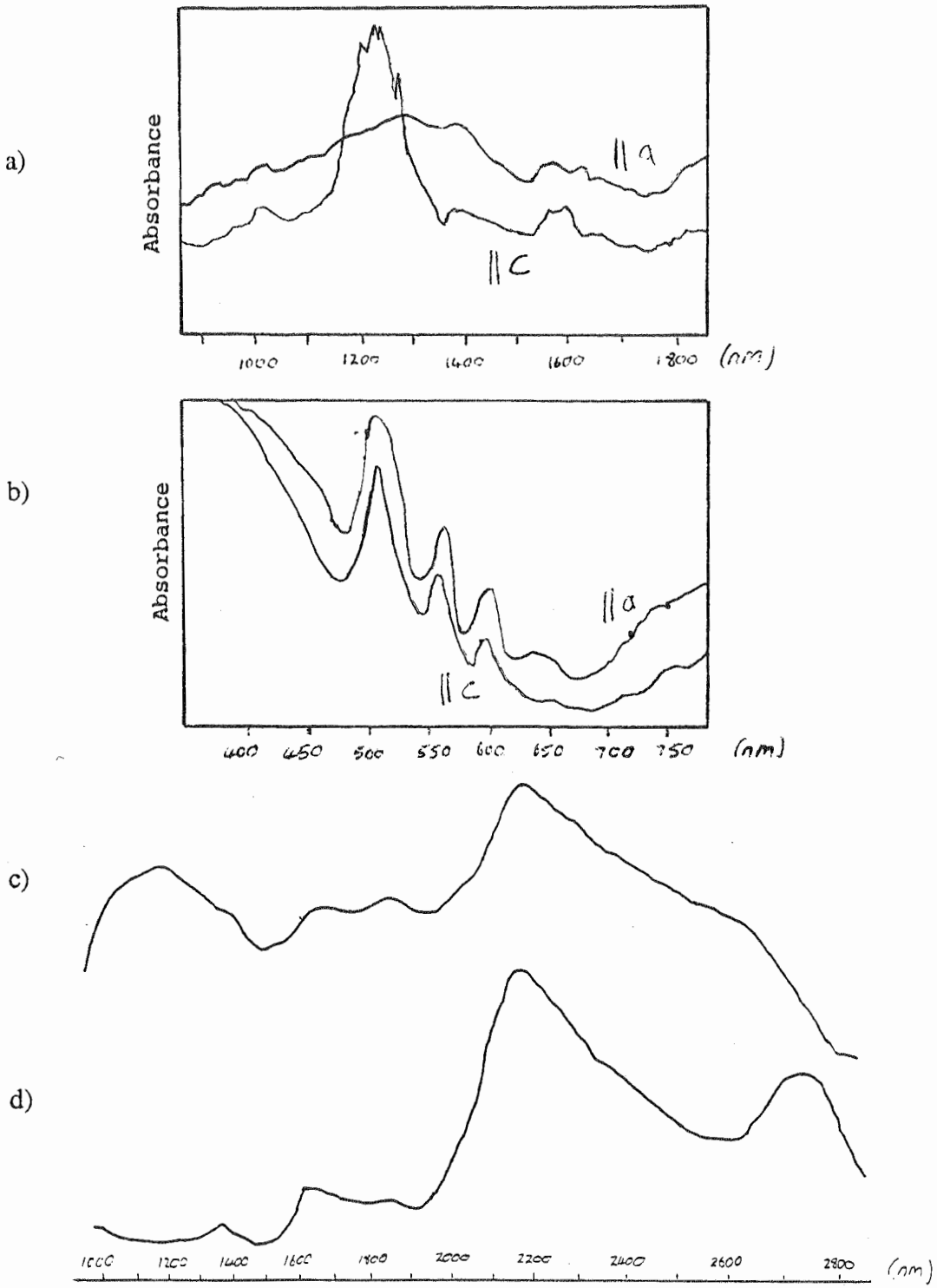

Figure 3.1 : polarised electronic spectra for $(enH_2)_2Zn[Cu]Br_6$

(a) d - d region (b) charge - transfer region

(c) powder reflectance spectrum for $(enH_2)_2Zn[Cu]Br_6$

(d) powder reflectance spectrum for $(enH_2)_2ZnBr_6$

3.5 Assignment of d-d transitions

For the $[CuBr_4]^{2-}$ ion in $(enH_2)_2Zn[Cu]Br_6$, the selection rules[24] for the assignment of d-d transitions are based upon a point group of C_{2v} symmetry. The deviation from D_{2d} symmetry being due to the inequivalence of the angles α and β [Figure 3.2]. The effective point group is in accordance with E.S.R. results, and the selection rules are shown in Table 3.1.

Table 3.1 Selection rules for $[CuBr_4]^{2-}$ in a C_{2v} point group

C_{2v} transition		polarisation axes
$^2A_1 (d_{x^2-y^2}) \rightarrow {}^2A_1 (d_{z^2})$	allowed	z
$^2A_1 (d_{x^2-y^2}) \rightarrow {}^2A_2 (d_{xy})$	forbidden	- -
$^2A_1 (d_{x^2-y^2}) \rightarrow {}^2B_1 (d_{xz})$	allowed	x
$^2A_1 (d_{x^2-y^2}) \rightarrow {}^2B_2 (d_{yz})$	allowed	y

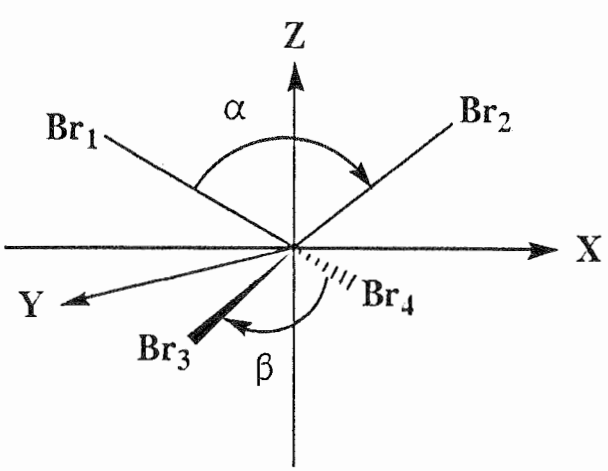

Figure 3.2 : definition of the angles α and β for the $[CuBr_4]^{2-}$ ion

From the single crystal spectra, the band at 8260 cm^{-1} is considerably more intense when the electric vector is parallel to the crystal c axis. The E.S.R. data gives the molecular projections made by a unit vector directed along this axis, as 0.5915x + 0.0y + 0.4085z. This band is therefore x and/or z polarised, which is consistent with the assignment as the $^2A_1(d_{x^2-y^2}) \rightarrow {}^2A_1(d_{z^2})$ transition. The weak band at 7100 cm^{-1} remains unpolarised, and is hence assigned to the formally forbidden transition $^2A_1 \rightarrow {}^2A_2$. At approximately 4000 cm^{-1} a band is observed which is significantly more intense when the electric vector is parallel to the crystal b axis. In this direction, a molecular projection of 0.0x + 1.0y + 0.0z implies that this band is y polarised, which is consistent with the lowest energy band being assigned to the $^2A_2 \rightarrow {}^2B_2$ transition. However, it must be stressed that single crystal studies cannot uniquely resolve d-d transitions below 6000 cm^{-1}. The formal assignment of this low energy band is therefore somewhat dubious.

3.6 Assignment of Charge-Transfer transitions

In T_d geometry, the twelve 4p valence orbitals of the bromine divide into 5 molecular orbitals, which split further in D_{2d} geometry, into six $p\pi$ and three $p\sigma$ molecular orbitals[25]. Of the nine possible ligand-to-metal charge transfer transitions, only five electric dipole allowed transitions are expected. The crystal spectrum of $(enH_2)_2Zn[Cu]Br_6$, shows 3 intense bands centred at 16950, 18180 and 19600 cm^{-1}, typical of charge-transfer transitions. From analogous studies[25,26], these are assigned to transitions as shown in Table 3.2.

On lowering the symmetry from D_{2d} to C_{2v}, as is the case when $\alpha \neq \beta$ [Figure 3.2], the E state is split, usually resulting in two bands being observed. The doublet expected from this splitting is assumed to be unresolved, as are the weak bands corresponding to the formally forbidden transitions $^2B_2 \rightarrow {}^2A_2$

Table 3.2 Selection rules for $[CuBr_4]^{2-}$ in a D_{2d} point group

D_{2d} transition	polarisation axes	energy (cm^{-1})
$^2B_2 (d_{xy}) \rightarrow {}^2A_1 (d_{z2})$	z	19600
$^2B_2 (d_{xy}) \rightarrow {}^2B_1 (d_{x2-y2})$	forbidden	16950
$^2B_2 (d_{xy}) \rightarrow {}^2E_1 (d_{xz},d_{yz})$	x,y	18180

and $^2B_2 \rightarrow {}^2B_2$. Regrettably, no significant polarisations were observed in this region, and hence these assignments cannot be considered as conclusive as those for the d-d spectrum.

3.8 Summary

Having determined the electronic spectral transition energies, it is now appropriate to correlate these transitions with the geometric structure of the guest $[CuBr_4]^{2-}$ ion. For the purpose of this work, the d-d transitions are the most valuable and informative. This by no means implies that the charge-transfer transitions are of only purely academic interest. Numerous studies[27] have focussed on these transitions alone, particularly for structure determination of the active copper site in ' blue ' proteins[25,28]. For many compounds of this class, all the possible d-d transitions are observed[28] at energies below 12000 cm^{-1} . Thus, the dominant *visible* spectral features have been attributed to charge-transfer transitions. The detailed interpretation of the electronic spectrum of these blue copper sites has given further insight into structural variations among similar sites in other proteins.

Since the d-d region for $(enH_2)_2Zn[Cu]Br_6$ is relevant to consideration of the metal-ligand bonding and analysis of the E.S.R spectra, a comprehensive analysis of the charge-transfer transitions is beyond the scope of this project.

CHAPTER 4.

BONDING PARAMETERS AND STRUCTURE

4.1 Introduction

A problem often encountered in the ligand-field analysis of optical and E.S.R spectra concerns the choice of an appropriate model. Ideally, the model should be capable of treating complexes with any coordination number and geometry, without an undue degree of parameterization, and should give a relationship between chemical bonding and the parameters, which is chemically reasonable.[29] The Angular Overlap Model (AOM)[30,31,32] seems to satisfy these criteria, and will subsequently be used in the interpretation of the bonding and geometry of the guest $[CuBr_4]^{2-}$ ion. It is therefore pertinent at this point to give a brief overview of this model.

4.2 The Angular Overlap Model

In parameterising the effects of ligands on a central transition metal ion, the (AOM) exploits two assumptions, these being[33]:

(1) the energy change $\Delta E(d)$ of a particular d-orbital caused by bond formation with ligand orbitals, is given by the sum :

$$\{F(d,\sigma)\}^2 e_\sigma + \{F(d,\pi_x)\}^2 e_{\pi x} + \{F(d,\pi_y)\}^2 e_{\pi y}$$

where F is the fraction of the total overlap integral

(2) the energy change of a particular d-orbital, caused by the coordination of several ligands, is the sum of the effects from each ligand.

Although it is not possible to prove these assumptions rigorously, they are justified by successful application of the model.

Consider the interaction of a metal d_z2 orbital and a ligand p_z orbital. This gives the secular determinant[33] :

$$\begin{array}{c|cc|} & d_z2 & p_z \\ d_z2 & \langle d_z2\,|H|\,d_z2\rangle - E & \langle d_z2\,|H|\,p_z\rangle - E\langle d_z2|p_z\rangle \\ p_z & \langle p_z\,|H|\,d_z2\rangle - E\langle d_z2|p_z\rangle & \langle p_z\,|H|\,p_z\rangle - E \end{array}$$

with the solution yielding the energies of the two molecular orbitals. A convenient orthogonal basis function permits the determinant to be written as[33] :

$$\begin{vmatrix} H(z^2,z^2) - E & H(z^2,p_z) \\ H(p_z,z^2) & H(p_z,p_z) - E \end{vmatrix}$$

Solving this, the energy change in the d_z2 orbital is given as[33] :

$$\Delta E(z^2) = \frac{H(z^2,p_z)^2}{H(z^2,z^2) - H(p_z,p_z)}$$

This can be simply extended to the general case for any metal (M) - ligand (L) interaction, giving :

$$\Delta E = \frac{(H_{ML})^2}{H_{MM} - H_{LL}}$$

The Wolfsberg-Helmholz approximation for off-diagonal elements states[34] :

$$H_{ML} = kG_{ML}\frac{(H_M - H_L)}{2}$$

where the group overlap integral G_{ML} divides into an angular part F_{ML} and a radial factor S_{ML}, known as the diatomic overlap integral. Thus :

$$\Delta E = \frac{(H_{LL})^2}{H_{MM} - H_{LL}} \cdot (G_{ML})^2$$

Introducing the AOM nomenclature[33], we get :

$$\Delta E = e_x(F_{ML})^2$$

where x = σ or π, and thus the parameter e_x is defined as :

$$e_x = \frac{(H_{LL})^2}{H_{MM} - H_{LL}} \cdot (S_{ML})^2$$

Adding the effects of all ligands together allows the overall energy changes of all d orbitals to be calculated.

For geometrical purposes, the position of each ligand must be specified by three angle η, ϕ and φ[33] as shown in Figure 4.1.

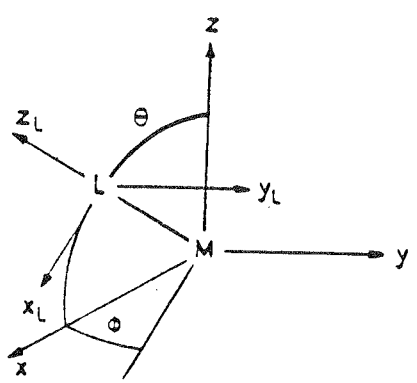

Figure 4.1 : specification of ligand positions for AOM

The position of a ligand L on the surface of a sphere surrounding the central metal ion can be characterised by η and ϕ where η is the angle between the z axis and the metal ligand bond, while ϕ is the angle between the x axis and the projection of the metal ligand bond onto the xy plane. The purpose of φ is to realise the alignment of the x and y axes of the ligand with the x and y axes of the metal. This is accomplished from rotation by φ about the z axis of the ligand which lies along the metal ligand bond. However, for so-called linearly ligating ligands such as Br^-, φ may have an arbitrary value, and hence is chosen to be 0^o for simplicity. This effectively means that the π interaction may be described using a single parameter

e_π, as opposed to components parallel and perpendicular to the plane of bonding.

A refinement of the AOM which is pertinent to this work, relates to the fact that, since the parameters e_σ and e_π are dependent on orbital overlap, bondlength variations will consequently have an effect. An $(R_{ML})^{-5}$ dependence has been proposed[35] (where R_{ML} = metal - ligand bond length) and has improved the transferability of parameters between different systems.

4.3 Calculation of geometry for the doped $[CuBr_4]^{2-}$ ion

It is necessary to determine optimal values for the parameters e_σ and e_π in order to evaluate the geometry of the doped $[CuBr_4]^{2-}$ ion. This optimisation routine has been automated in the FORTRAN computer program CAMMAG[36] (see Appendix B). A hypothetical structure for the guest ion is used which is then further manipulated to obtain a set of best-fit parameters. Initially, it is assumed that the geometry of the guest $[CuBr_4]^{2-}$ ion in $(enH_2)_2Zn[Cu]Br_6$ will be closely approximated by that of the distorted tetrahedral ion in bis-(ethylenediammonium-monobromide) tetrabromocuprate[16] $(enH.HBr)_2CuBr_4$. For this compound the relevant crystal data are shown in Table 4.1, with the ligand numbering system depicted in Figure 4.2.

Table 4.1 Crystallographic data for $(enH.HBr)_2CuBr_4$

space group	bond lengths		bond angles		unit cell	
$P2_1/m$	Cu - Br (1)	2.426	α	141.1	a	6.78
	Cu - Br (2)	2.426	β	118.1	b	20.15
	Cu - Br (3)	2.447			c	6.33
	Cu - Br (4)	2.330.				

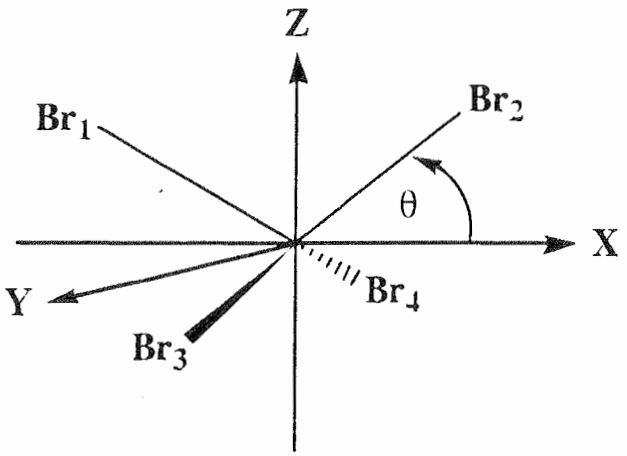

Figure 4.2 : ligand numbering in the $[CuBr_4]^{2-}$ unit

Initial values for e_σ and e_π were taken from those previously calculated for Cs_2CuBr_4[37], incorporating the adjustment for variations in bond length as described in section 4.2. The result is a set of calculated d-d transitions as shown in the first column of Table 4.2. As can be seen, the agreement with experimentally observed transitions is poor, so it is now necessary to refine the test data for optimum agreement.

The energies of the d-d transitions will vary as a function of

(1) continuous distortion from a square planar to a regular tetrahedral geometry; and

(2) the extension of one metal-ligand bond of an initially regular tetrahedral.

Previous studies[15] have shown that the dominant influence on d-d transition energies is a bond angle perturbation, rather than a bond length perturbation. Figure 4.3 shows a plot of the change in d-d transition energies against the distortion angle (θ)[38], defined pictorially in Figure 4.2. This plot actually relates to the $[CuCl_4]^{2-}$ ion, but the slopes of the lines can give an overall trend which can then be extended to the case for the $[CuBr_4]^{2-}$ ion..

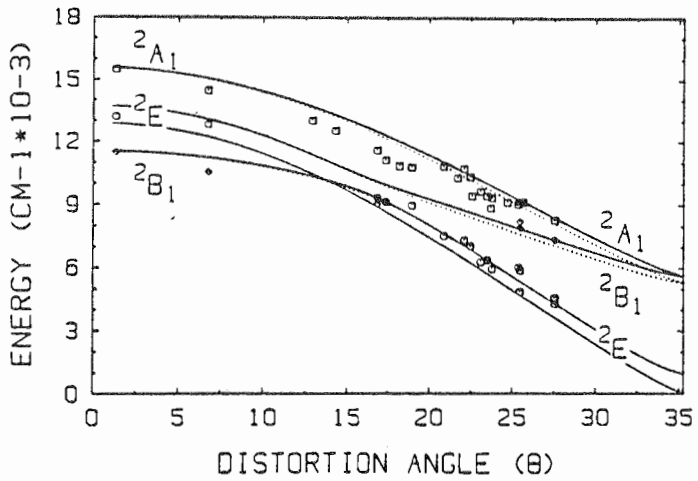

Figure 4.3 : plot of d-d transition energies against distortion angle

From this new data, an increase of ~2° for θ, corresponding to decreases in α and β of 2°, decreases the calculated transition energies to the values shown in column two of Table 4.2. The agreement with experiment now is well within expected limits.

Table 4.2 Optimised d-d transitions from CAMMAG

(1) - without correction for distortion angle

(2) - adjusting distortion angle by ~ 2°

observed	calculated (1)	calculated (2)
8260	8303	8103
(7100)	7971	7571
5400	6129	5329
3800	4124	3724

all values in cm^{-1}

4.4 Discussion

The angles α and β present in the guest $[CuBr_4]^{2-}$ ion have been calculated to be ~139° and ~116° respectively while the corresponding angles in the host $[ZnBr_4]^{2-}$ ion are 123.3° and 107.6°. From Table 4.3 it can be seen that the ratio α : β is approximately the same, when comparing the guest and host species. In addition, the magnitude of the deviation of α from a regular tetrahedral geometry (where $\alpha = \beta = 109.5°$) is about twice as much for the copper ion as it is for the zinc host. The preference for the copper ion to adopt its own geometry, rather than that of the host, is obvious.

Table 4.3 Distortion angles in the guest and host ions

species	α	β	$\alpha - \beta$	$T_d - \alpha$	$T_d - \beta$
$[CuBr_4]^{2-}$	~139	~116	23	30	7
$[ZnBr_4]^{2-}$	123.3	107.6	16	14	2.5

CHAPTER 5

ELECTRON SPIN RESONANCE SPECTROSCOPY

5.1 Theoretical Outline

The theory of Electron Spin Resonance (E.S.R) is well described elsewhere[39,40], however a brief introduction to the aspects relevant to this work is given below.

Copper in oxidation state (II) has a d^9 electron configuration, and thus has one unpaired electron. The spinning of this electron about its own axis creates spin angular momentum, and also gives rise to a rotating magnetic dipole or magnetic moment. In addition to this, the copper nucleus itself possesses a non-zero spin angular momentum and magnetic moment. The primary concern in an ESR experiment is the absorption of microwave radiation in an externally applied magnetic field.

In the absence of a magnetic field, the energy levels of the ground state are coincident or degenerate[39]. However, under the influence of a magnetic field, this degeneracy is lifted, and the energy levels are split. The measured transitions between these levels form the basis of an ESR spectrum. The resonance condition for such transitions can be characterised by the tensor quantity **g**, as shown by equation 5.1[39] :

$$g = h\upsilon / \beta H_r \qquad (5.1)$$

where h is Planck's constant, β is the Bohr magneton, H_r is the resonant magnetic field and υ is the frequency of the microwaves irradiating the sample. For anisotropic systems, which includes the compounds being studied in this work, the magnetic moment is a function of the orientation of the system within the magnetic field. Thus, in order to succinctly specify the **g** tensor, three mutually perpendicular directions (principal axes) must be defined, together with the

components of the **g** tensor along these directions (principal values).

Experimentally, it is often observed that an ESR signal splits into a number of lines whose intensities are in (or close to) simple integral ratios, and which are disposed in a centro-symmetric pattern[40]. This effect arises from the interaction of unpaired electron spins with the nuclear magnetic moment of the metal, and is known as hyperfine structure. This hyperfine interaction is also orientation dependent, and must therefore be defined as a tensor quantity, similar to **g**. The term hyperfine 'splitting' is used to designate the line spacing observed in an ESR spectrum as a result of hyperfine coupling. To allow a conversion of the hyperfine splittings, measured in gauss, to a value in energy units, the hyperfine coupling constant **A** is introduced, as defined in equation 5.2[39] :

$$A\ (cm^{-1}) = C\left(\frac{g}{g_e}\right) a\ (gauss) \qquad (5.2)$$

where g is the measured g value, g_e is the 'free electron' g value[39], and C is a constant, depending on the chosen units.

A further interaction to be considered is that of the unpaired electron with the nuclear moment of the ligands. This results in superhyperfine structure, and the values of these couplings are usually determined from line-shape simulation studies. The fact that the superhyperfine coupling is a tensor quantity too, makes the spectrum difficult to interpret as we now have multiple sets of principal values and axes.

5.2 Experimental

The E.S.R spectra were recorded on a ' JEOL JES FE3X ' Electron Spin Resonance spectrometer operating at X-band frequency. Analogous studies[10] have shown that room temperature spectra consist of relatively broad, weak signals, and consequently such measurements were not pursued. Therefore, all measurements were conducted at 120 K, this being the lowest temperature obtainable when using

the variable temperature unit. For the $(enH_2)_2Zn[Cu]Br_6$ system, an insertion dewar allowed the spectrum to be recorded at 77K.

Single crystals were mounted on a flat, vertical face shaped from the end of an opaque quartz rod [Figure 5.1 (a)]. The polarising microscope was used, to align a crystal axis parallel to the longitudinal axis of the quartz rod. A small spot of α, α' - diphenyl - β - picrylhydrazyl (DPPH) was placed near the crystal, acting as an internal standard with an accurately known g-value[39] (2.0036). The rod was then placed inside a clear quartz E.S.R. tube and sealed from the atmosphere. This tube was itself placed in a circular rotatable jacket having a calibrated scale of 0 to 360°. The position of the quartz tube within the jacket could be adjusted via a teflon washer, ensuring the crystal was correctly positioned within the cavity.

The rod was rotated through 180°, with respect to the magnetic field, and separate spectra were recorded at 15° intervals. This procedure was repeated twice, with the crystal in different orientations, so that orthogonal crystal faces alligned along the quartz rod [Figure 5.1 (b)]. Hence, each complete E.S.R. measurement consisted of three mutually perpendicular rotations.

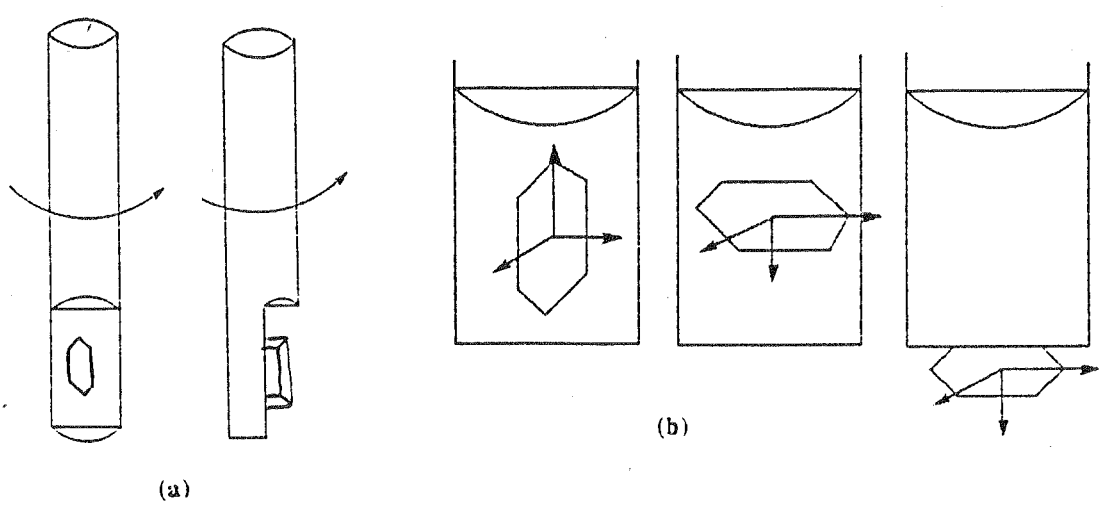

Figure 5.1 : a) mounting crystals on quartz rod

b) three rotation planes of the crystal

5.3 Single Crystal E.S.R. Results

Single crystal spectra were recorded for the pure copper compound $(enH_2)CuBr_4$ and for the doped systems $(Me_4N)_2Zn[Cu]Br_4$, $Rb_3Zn[Cu]Br_5$, $Cs_2Zn[Cu]Br_4$ and $(enH_2)_2Zn[Cu]Br_6$

For $(enH_2)CuBr_4$, a single symmetrical signal was observed for all three rotations [Figure 5.2 (a)], which reached a maximal and minimal shift from the DPPH when the magnetic field was applied along a crystal axis. Within each rotation, the signal was observed to be orientation dependent, meaning that the shift from the DPPH and the intensity were unique to the orientation in the magnetic field. Plots of measured values of g^2 against rotation with respect to the magnetic field (η) are given in Figure 5.2 (b)

Figures 5.3 (a) - (d) show two examples of the recorded spectra for each of the doped compounds studied. At 120 K, a significant hyperfine coupling was resolved for $(enH_2)_2Zn[Cu]Br_6$, while for $Rb_3Zn[Cu]Br_5$, the resolution was considerably less. In the case of $(Me_4N)_2Zn[Cu]Br_4$ and $Cs_2Zn[Cu]Br_4$, the spectra for all three rotations showed little structure.

On the basis of these observations, it was decided that further investigation of $(enH_2)_2Zn[Cu]Br_6$ would be most beneficial. Hence, a complete set of spectra were measured for this compound at 77 K, with the aim of achieving a greater resolution. This proved successful, and examples of the spectra are shown in Figure 5.4 (a), with the corresponding plots of g^2 against (η) shown in Figure 5.4 (b).

5.4 Treatment of E.S.R. Data

The following sub-sections describe the calculation of the E.S.R parameters from the measured spectra. The discussion will focus mainly on $(enH_2)_2Zn[Cu]Br_6$, as this gave the best resolution and thus the most informative spectra. It should be noted that some of the more general comments made will have relevance to the preliminary studies of the other doped systems.

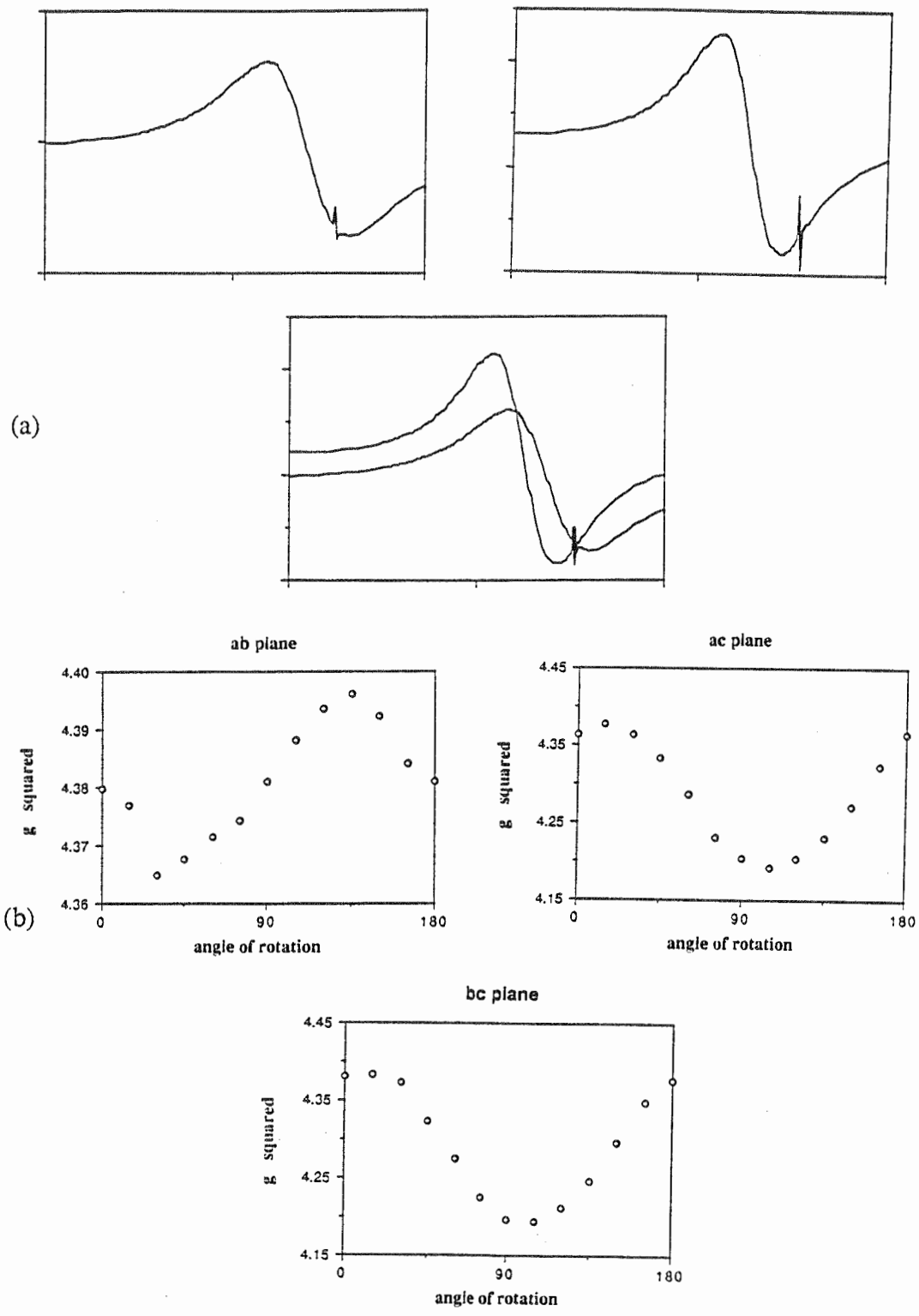

Figure 5.2 : a) examples of E.S.R spectra for $(enH_2)CuBr_4$ at 120K

* horizontal scale measured in gauss

b) plots of g^2 against angle of rotation (η) for $(enH_2)CuBr_4$

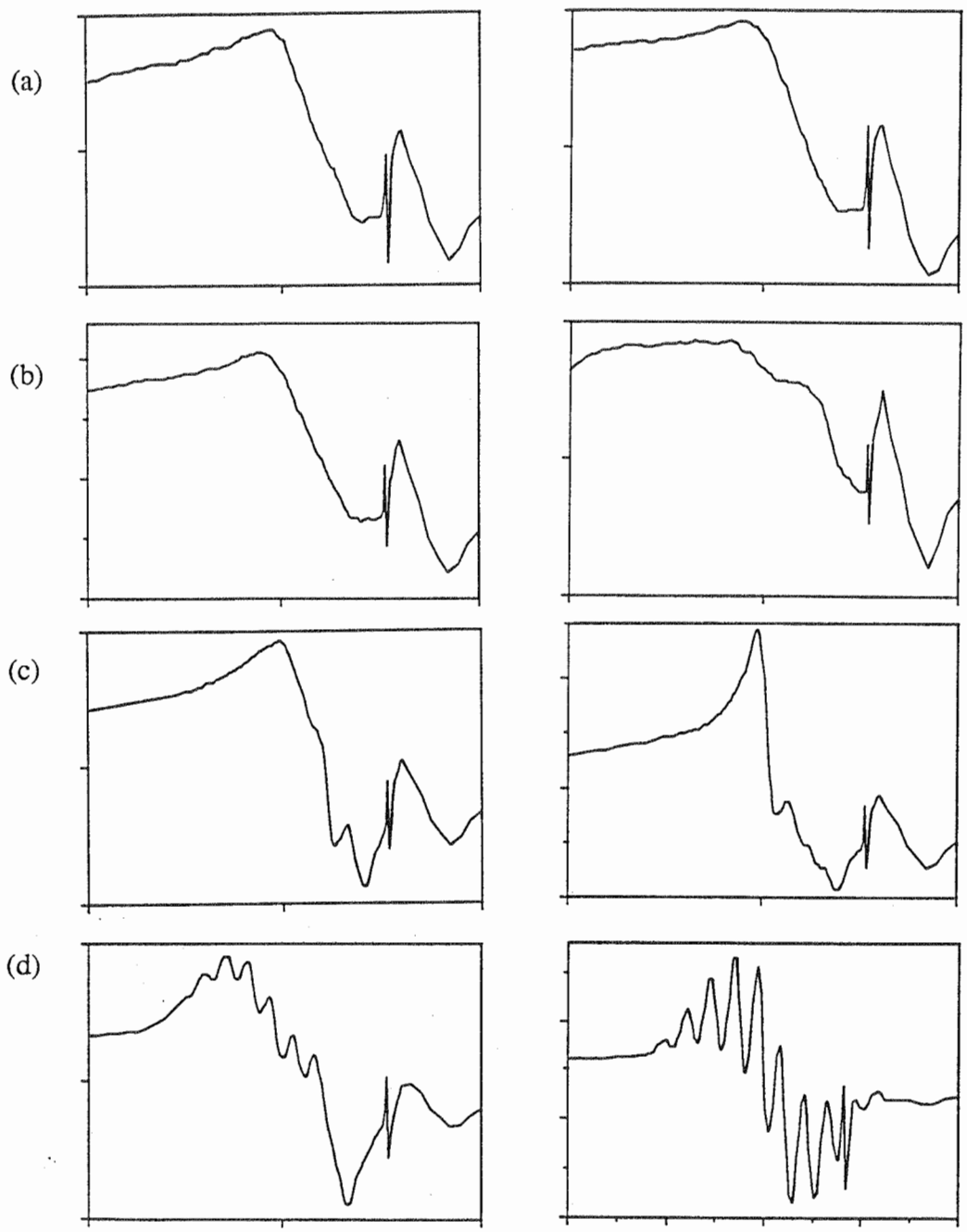

Figure 5.3 : examples of single crystal E.S.R. spectra measured at 120 K

a) $Cs_2Zn[Cu]Br_4$

b) $(Me_4N)_2Zn[Cu]Br_4$

c) $Rb_3Zn[Cu]Br_5$

d) $(enH_2)_2Zn[Cu]Br_6$

* horizontal scale measured in gauss

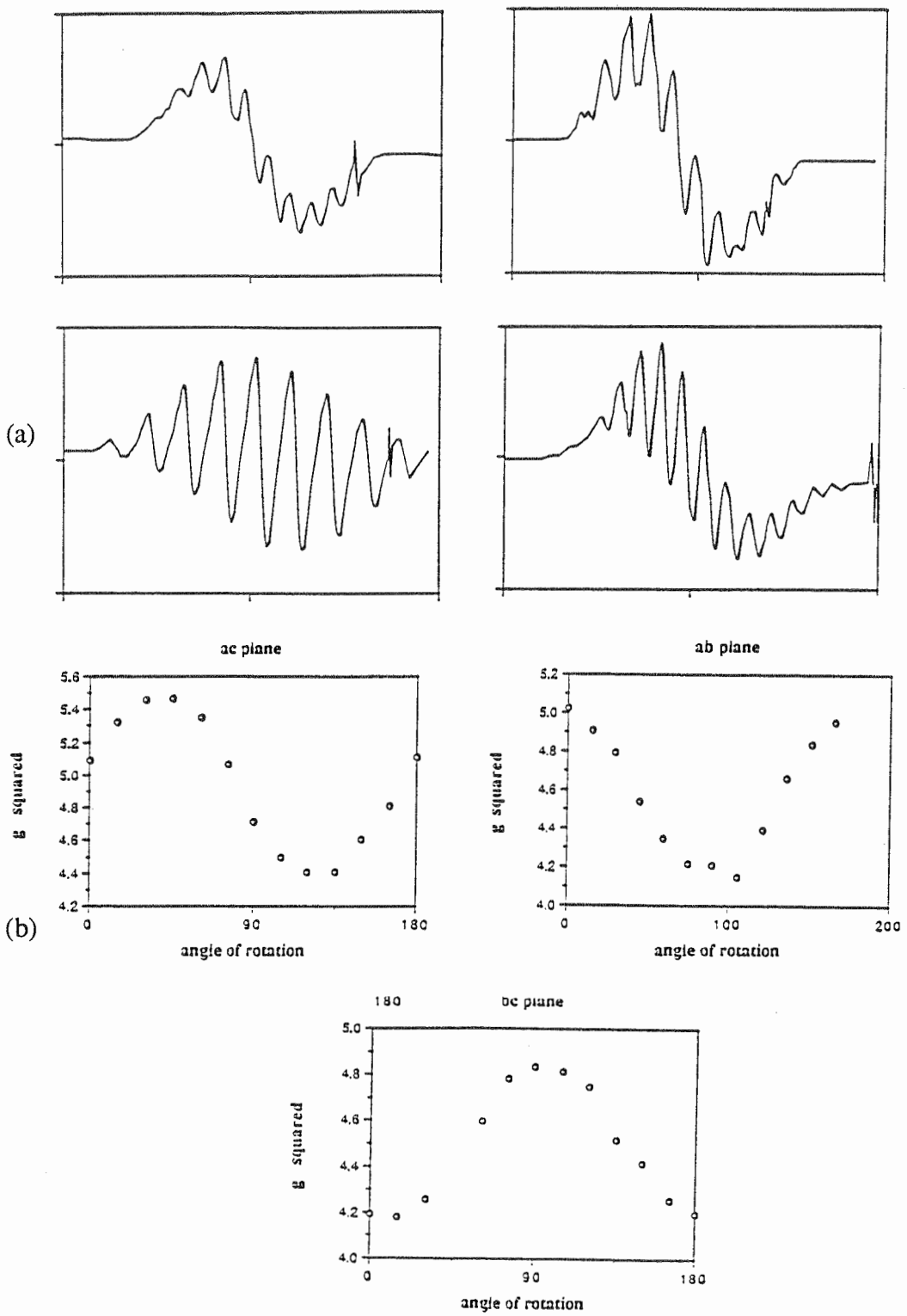

Figure 5.4 : a) examples of E.S.R spectra for $(enH_2)_2Zn[Cu]Br_6$ at 77 K

* horizontal scale measured in gauss

b) plots of g^2 against angle of rotation (η) for $(enH_2)_2Zn[Cu]Br_6$

5.4.1 Calculation of Molecular g Tensors

Firstly, a set of molecular axes were defined, as shown in Figure 5.5, consistent with the calculations presented in the previous chapter. Thus, the z axis bisects the angle α, the x axis lies in the plane of α and is normal to z and the y axis is orthogonal to z and x. The principal g values were derived from the measured crystal g values using the FORTRAN computer program ' GTENSOR ' (see Appendix B). This essentially describes the g value obtained from each experimental signal by an equation of the form[41] :

$$g^2 = x^2 g_{xx}^2 + y^2 g_{yy}^2 + z^2 g_{zz}^2 + 2xy g_{xy}^2 + 2yz g_{yz}^2 + 2xz g_{xz}^2 \qquad (5.3)$$

where x, y and z are the direction cosines between the magnetic field vector and the principal axes defined. The g-tensor elements g_{xx} ,g_{yz} etc. are determined by a least-squares procedure, with the diagonalization[41] of this tensor resulting in the principal **g** values and the respective directions.

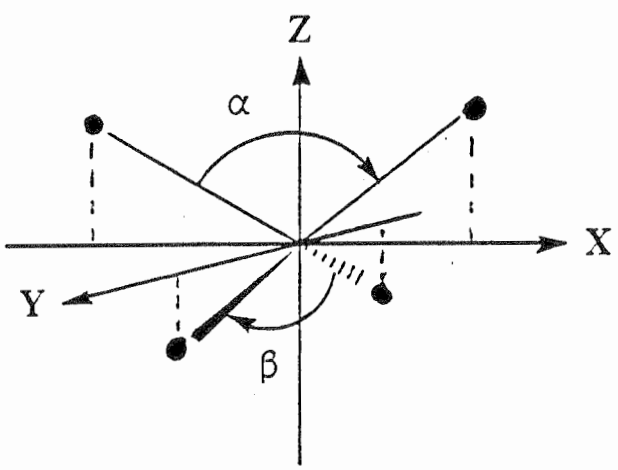

Figure 5.5 : Definition of molecular axes

Table 5.1 shows the principal g values obtained for $(enH_2)_2Zn[Cu]Br_6$, while in Figure 5.6 ,we can see that the alignment of the **g** tensor axes with the molecular axes is excellent.

Table 5.1 principal g values for $(enH_2)_2Zn[Cu]Br_6$

g_x	g_y	g_z
2.0429	2.0912	2.3409

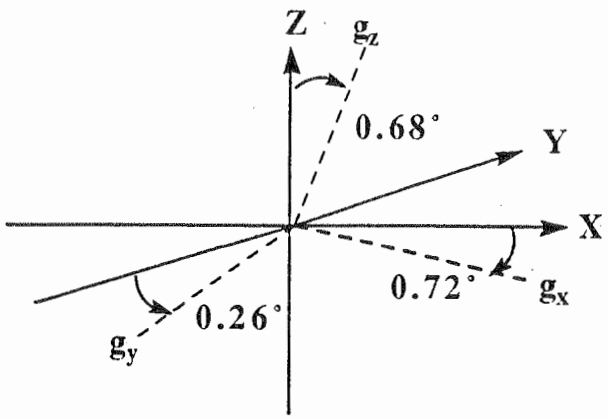

Figure 5.6 Orientation of g tensor axes with respect to the molecular axes

5.4.2 Calculation of hyperfine and superhyperfine tensors

At 120K, a significant hyperfine and superhyperfine coupling was resolved for $(enH_2)_2Zn[Cu]Br_6$, with the resolution improving upon cooling to 77K [Figure 5.4].

The hyperfine coupling arises from the interaction of the unpaired d electron with the non-zero nuclear spin of the copper. Therefore, an isolated copper nucleus ($^{63}Cu = 69\%$, $^{65}Cu = 31\%$)[42] with a nuclear spin $I = \frac{3}{2}$ will give an E.S.R. signal containing $2I + 1 = 4$ lines[39] [Figure 5.7 (a)]. It may be assumed that the axes of this tensor coincide with those of the **g** tensor. The superhyperfine coupling is a measure of the interaction of the unpaired d electron with the nuclear spin ($I = \frac{3}{2}$) of each bromine. Thus, as ligands are introduced into the system, the simple 4 line signal for a lone copper ion will be further split into many more components, as is the case for $(enH_2)_2Zn[Cu]Br_6$. When the

superhyperfine coupling bears an integral relation to the hyperfine coupling, these additional patterns will interfere with one another, and thus produce a symmetrical pattern [Figure 5.7 (b)].

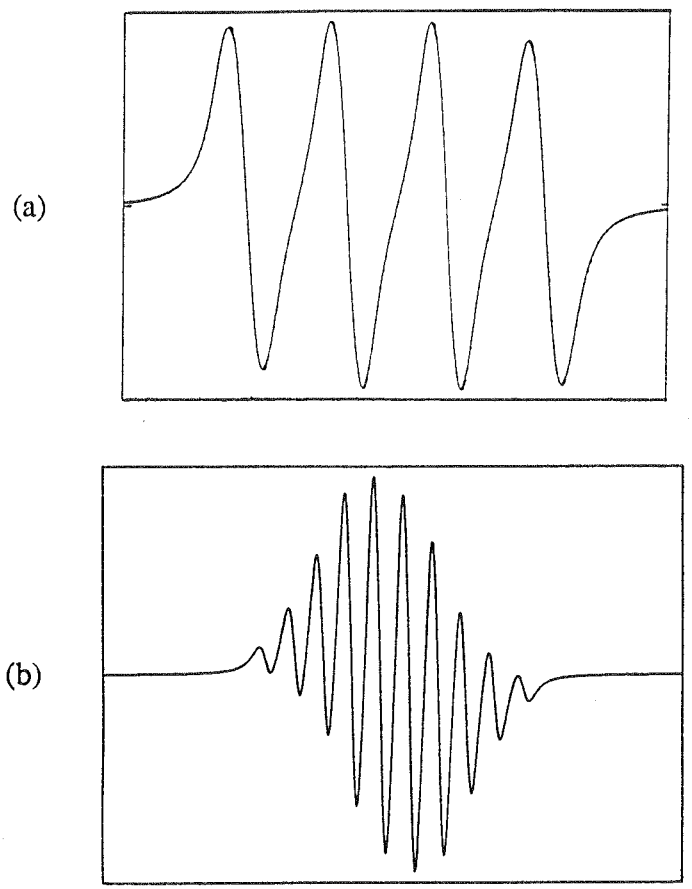

Figure 5.7 : (a) hyperfine splitting
(b) superhyperfine splitting

Line shape simulation studies were used to determine the tensor parameters. Previous studies on comparable systems[10] were used to estimate initial values which were adjusted until the computer generated spectra duplicated the observed spectra.

The situation for $(enH_2)_2Zn[Cu]Br_6$ is complicated by the marked difference between the angles α and β [Figure 5.8], which necessitates the demarcation of two different types of bromine atom. In this work, the focus of

attention is on the type 2 bromine atoms, denoted Br_2, which are defined to line in the y z plane, with the z axis bisecting the angle α.

The axes defining the principal directions of the superhyperfine tensors are denoted x', y' and z', with z' approximately along the Cu - Br bond, x' parallel to the x molecular axis and y' in the zy plane.

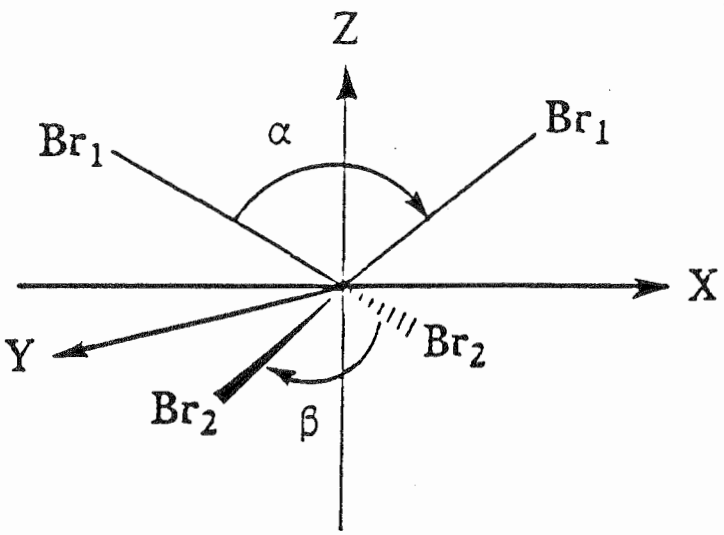

Figure 5.8 : definition of atom types

To obtain a set of self-consistent values for the hyperfine and superhyperfine tensors, the three spectra shown in Figure 5.9 were chosen for the simulation study . Spectrum #1 corresponds to the magnetic field being directed along the y molecular axis, with spectrum #2 measured along the z molecular axis. From analysis of the relevant g value data, it was determined that spectrum #3 results from the magnetic filed directed at an angle of ~45^{o} to the z (and y) axis.

The separation of the component peaks may be used to determine approximate values for the hyperfine tensor, with the value along 45^{o} determined from those along the molecular y and z axes.

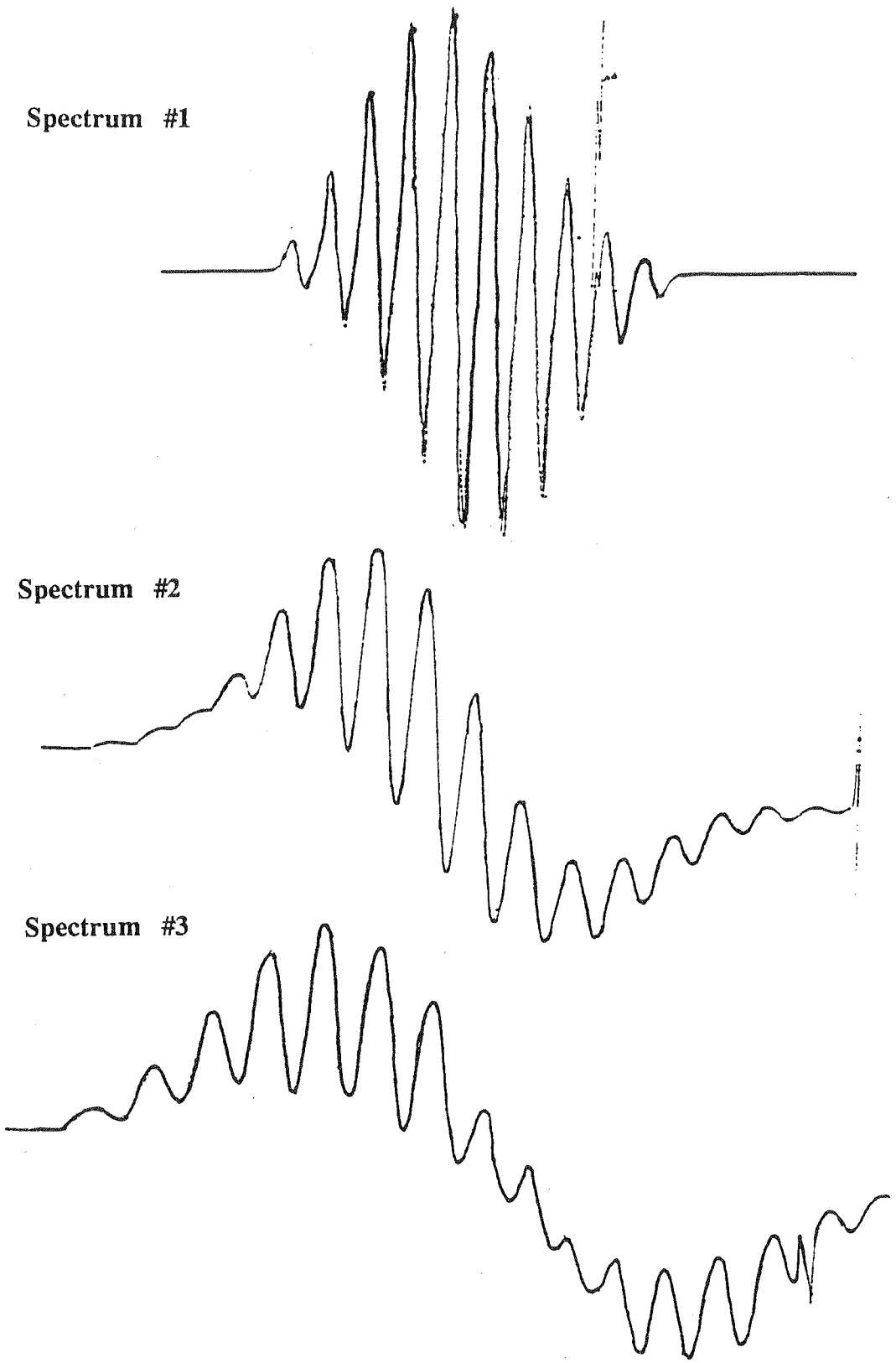

Figure 5.9 : experimental E.S.R spectra chosen for simulation

For the spectrum measured along the molecular z axis, the equations[8] :

$$A_z2 = A_{z'}2 \cos^2\theta + A_{x'}2 \sin^2\theta \qquad (5.4a)$$

$$A_y2 = A_{z'}2 \sin^2\theta + A_{x'}2 \cos^2\theta \qquad (5.4b)$$

relate the measured superhyperfine values to the principal superhyperfine values, where θ is the angle between the z' superhyperfine axis and the z molecular axis. These can easily be extended to correlate with the other two spectra, thus giving a set of equations to define possible values for θ and the principal superhyperfine parameters.

The main problem encountered here is that for each pair of equations, there are *three* unknown values. A visual interpretation of the spectrum can provide an idea of the number of nuclei coupling in order to produce the interference pattern observed.

For spectrum #1 (along y), a 10-line pattern is observed, as is expected for the coupling of *three* equivalent nuclei, all with spin $I = \frac{3}{2}$. This splitting may be rationalised by the coupling of the copper nucleus with the 'type 2' bromine nuclei [Figure 5.8 (a)]. Spectrum #2 (along z) shows a 16-line pattern, with a separation of approximately 60 gauss between each pair of lines. This is consistent with an equivalent coupling of *five* nuclei, i.e the splitting due to all four bromine nuclei equals that for the copper nucleus. For the third spectrum (45^o), a 15-line pattern is displayed, which cannot be justified by coupling of *equivalent* nuclei. One possible explanation for this pattern is the equivalent coupling of the copper nucleus with the two 'type 1' bromine nuclei, plus a coupling of *one* 'type 2' bromine nucleus having a value twice that of the former.

A more quantitative explanation for these observed patterns is displayed in Figure 5.10. By means of a ' stick ' diagram, this shows the coupling of three equivalent nuclei, resulting in the 10 line interference pattern with relative peak intensity ratios of 1 : 3 : 6 : 10 : 12 : 12 : 10 : 6 : 3 : 1 .

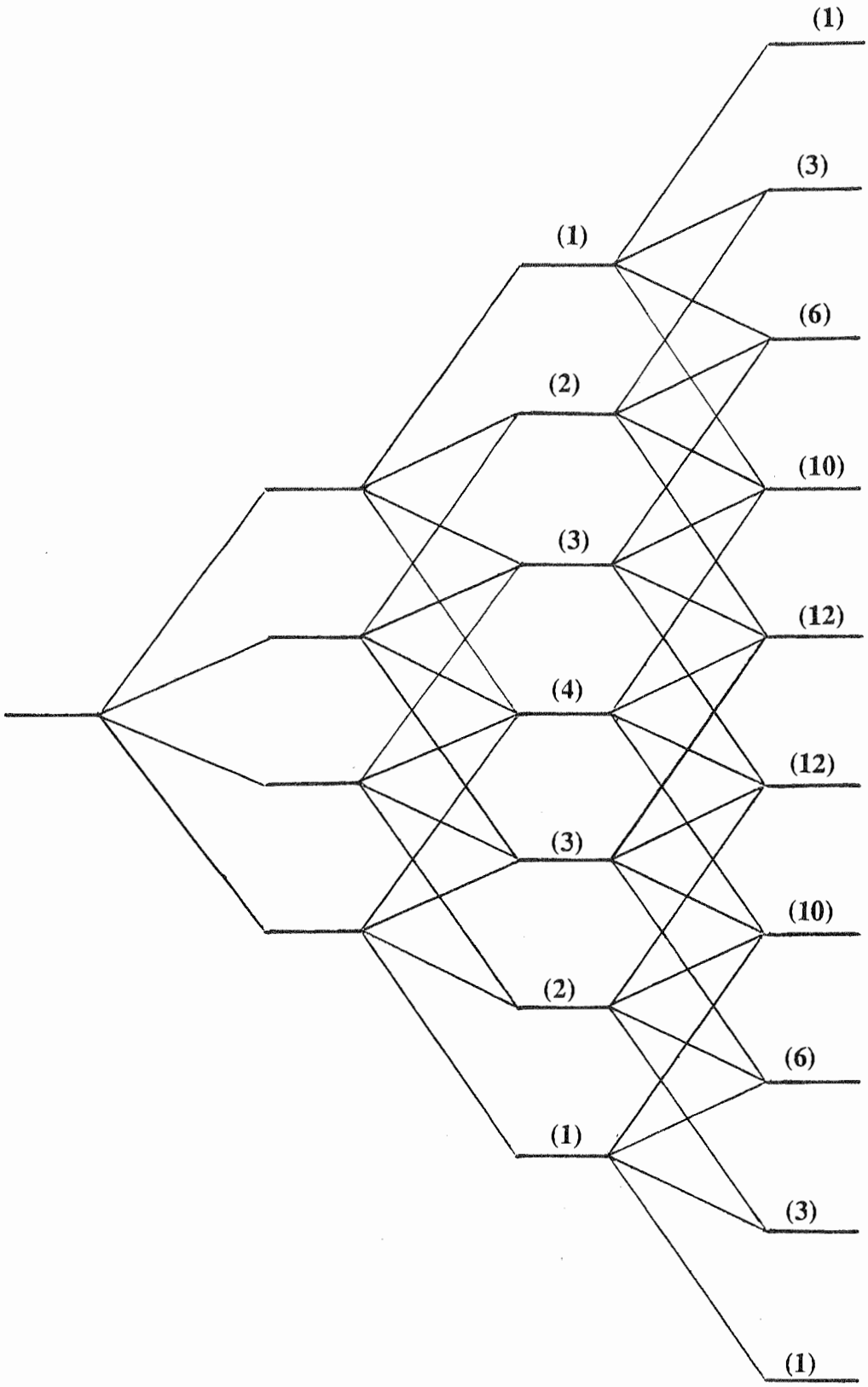

Figure 5.10 : splitting pattern observed for three equivalent nuclei

* values in parentheses are relative peak intensities

Combined with analogous studies[10], the previous information may provide a set of 'starting values' for the two tensors and θ. These are refined so that firstly, the pair of equations relevant to each spectrum are satisfied, and secondly, the computer simulated spectrum generated from these values replicates the observed spectrum. Such constraints prove to be quite rigorous, permitting values in a range of only $\pm$ 3 gauss which is well within experimental error.

5.5 Summary

The 'best-fit' values for the hyperfine and superhyperfine tensors are shown in Table 5.2, while Figure 5.11 displays the orientation of the axes for the latter parameter. For comparison, the computer-generated spectra are shown in Figure 5.12 .

Table 5.2 E.S.R data for $(enH_2)_2Zn[Cu]Br_6$

axis	g value	hyperfine coupling (x 10^{-4} cm^{-1})	superhyperfine coupling (x 10^{-4} cm^{-1})
x	2.0429 $\pm$ 0.0003	~46 $\pm$ 3	~0.0 $\pm$ 3
y	2.0912 $\pm$ 0.0003	49.2 $\pm$ 3	~0.0 $\pm$ 3
z	2.3409 $\pm$ 0.0004	43.9 $\pm$ 3	72.3 $\pm$ 3

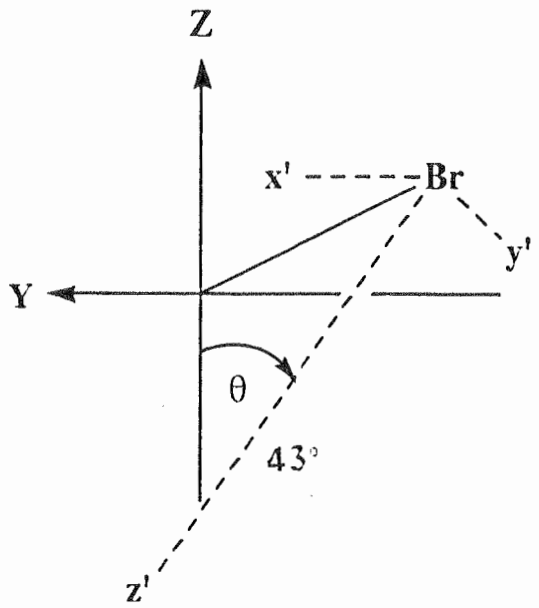

Figure 5.11 : orientation of the superhyperfine axes with respect to the molecular axes

Unfortunately, symmetrical interference patterns were not observed for the E.S.R spectrum measured along the molecular x axis. It is therefore difficult to make an initial guess of the hyperfine copper and bromine parameters, and as a result, values for the hyperfine and superhyperfine tensors cannot be confidently reported. It must be stressed that this task is by no means impossible, and with more time, self-consistent values could be found to incorporate spectra measured along all three axes.

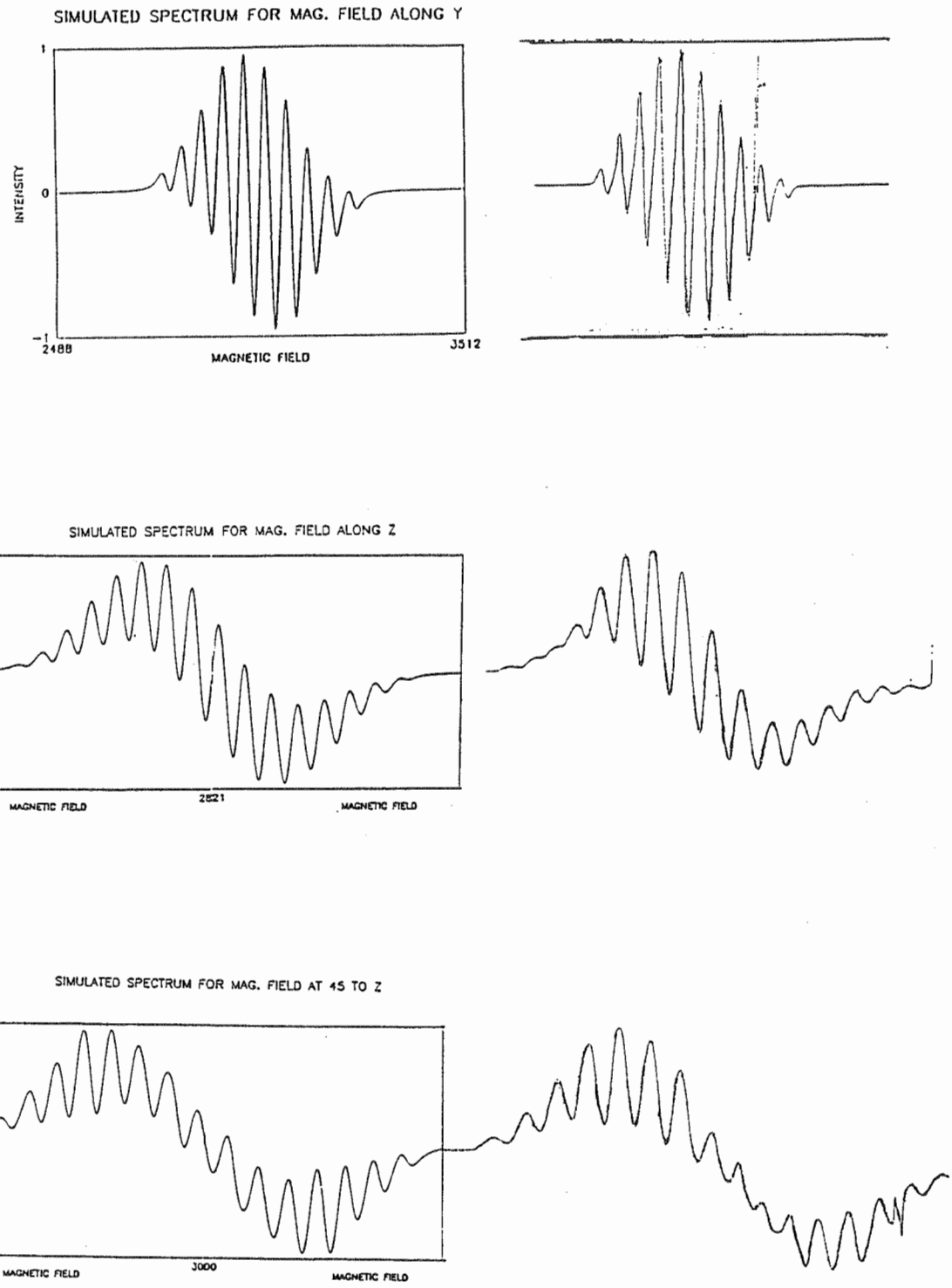

Figure 5.12 : observed (right) and computer-generated (left) E.S.R spectra

CHAPTER 6.

INTERPRETATION OF E.S.R. RESULTS

6.1 Introduction

Having obtained the parameters from the E.S.R. measurements of the $(enH_2)_2Zn[Cu]Br_6$ system, it is now appropriate to present a comprehensive analysis of these results, with the aim of elucidating the bonding and geometry of the $[CuBr_4]^{2-}$ unit .

6.2 Covalency of the Cu - Br Bond

The values of the superhyperfine coupling constants relate to the proportion of time that the unpaired electron spends in the ligand bonding orbitals and thus permits a direct measure to be made of the covalency of the metal-ligand bond.

The principal superhyperfine values can be expressed in terms of an isotropic component $A_{S'}$, due to the occupancy of the bromine 4s orbital, and the anisotropic component $A_{p'}$ from occupancy of the 4p bromine orbital. This latter element may be further broken down, giving the contributions $Ap_{z'}$ and $Ap_{y'}$, which result from the bromine $4p_{z'}$ and $4p_{y'}$ orbitals overlapping with the copper d_{x2-y2} orbital. In addition, the unpaired electron density at the copper will give a small dipolar contribution denoted $A_{D'}$.

Expressions for the relationships[43] between the above parameters are shown in equations 6.1 (a) - (c) below. These have been extended from the case for an axially symmetric tensor[43] to the rhombic condition observed for $(enH_2)_2Zn[Cu]Br_6$.

$$A_{x'} = A_{s'} + 2A_{px'} - A_{pz'} - A_{D'} \qquad (6.1a)$$

$$A_{y'} = A_{s'} - A_{px'} - A_{pz'} - A_{D'} \qquad (6.1b)$$

$$A_{z'} = A_{s'} + 2A_{pz'} - A_{px'} + 2A_{D'} \qquad (6.1c)$$

The isotropic and dipolar terms may be related to the unpaired electron density in the 4s and 4p orbitals via[43] :

$$A_{s'} = \frac{16\pi\gamma\beta\beta_N}{3} f_{s'} |S(0)|^2 \qquad (6.2a)$$

$$A_{p'} = \frac{4\gamma\beta\beta_N}{5} f_{p'} \langle r^{-3p} \rangle \qquad (6.2b)$$

where $f_{s'}$ and $f_{p'}$ represent the fraction of time the unpaired electron spends in the bromine s and p orbitals respectively. In this work, however, we make use of an alternative procedure described by Morton and Preston[44]. Briefly, in this method, $|S(0)|^2$ and $\langle r^{-3p} \rangle$ are calculated in terms of the Hermann-Skillman wavefunction, as opposed to the Hartree-Fock wavefunctions which were considered unacceptable.

Solving equations 6.1 and 6.2, using the estimates[8] $A_{D'} \simeq 0.14 \times 10^{-4}$ cm^{-1} and $A_{px'} \simeq 0\ cm^{-1}$ gives :

$$A_{s'} \simeq A_{pz'} \simeq 26.34\ (\times 10^{-4})\ cm^{-1}$$

corresponding to occupations of the 4s and 4p orbitals of 0.25% and 9.7% respectively. This is equivalent to the unpaired electron spending about 40% of its time localised on the ligands.

Table 6.2 presents the results obtained for $(enH_2)_2Zn[Cu]Br_6$, along with the relevant values taken from the literature for various other systems.

The calculated ligand occupancy for $(enH_2)_2Zn[Cu]Br_6$ compares favourably with a value of ~50% obtained from a simplified interpretation of the orbital reduction parameters, and is greater, as expected, than that for the corresponding chloride complex.

For the first three compounds of Table 6.2, the general trend in moving from the bromide to the flouride complex is an increase in s orbital occupancy,

Table 6.2 Covalency of various $[CuX_4]^{2-}$ systems (X = F, Cl, Br)

compound	$f_{s'}$ (%)	$f_{p'}$ (%)	total occupancy (%)		ref.
			ligand	metal	
$(enH_2)_2Zn[Cu]Br_6$	0.25	9.7	40	60	this work
$(enH_2)_2Zn[Cu]Cl_6$	0.47	8.34	30	70	8
$Ba_2Zn[Cu]F_6$	0.5	6.2	27	73	45
$K_2Pd[Cu]Br_4$	0.21	11.6	47	53	10

corresponding to a decrease in the occupancy of the p orbital and thus a decrease in covalency. These observations are in complete agreement with the trend in electronegativities for the Fl^-, Cl^- and Br^- ions[5].

The $[CuBr_4]^{2-}$ unit in $K_2Pd[Cu]Br_4$ has a square-planar geometry[10], and as shown, an increase in covalency when compared with the distorted tetrahedral arrangement in $(enH_2)_2Zn[Cu]Br_6$. This is consistent with the fact that, for a square planar geometry, the lobes of the groundstate point directly along the Cu-Br bond. It is therefore reasonable to expect a greater overlap between the 4s and 4p orbitals and the groundstate. In the case of the distorted tetrahedral geometry in $(enH_2)_2Zn[Cu]Br_6$, the ligand 4s orbital is removed from the plane of the groundstate, resulting in a poorer overlap [Figure 6.1].

For the ligand $4p_z$ orbital, a similar decrease in overlap should occur when moving away from the groundstate plane. However, in this situation, the $4p_x$ orbital is now no longer orthogonal to the groundstate lobe, and thus overlap can occur. These considerations predict a decrease in $A_{||}'$ on moving toward a tetrahedral geometry, and a splitting of $A_{\perp}'$. This is entirely consistent with the

observed values of $A_{||}' = 123 \times 10^{-4}$ cm^{-1} and $A_{\perp}' = 27.9 \times 10^{-4}$ cm^{-1} for the planar compound, and $A_{z'} = 72.3 \times 10^{-4}$ cm^{-1} and $A_{x'} = A_{y'} \simeq 0$.

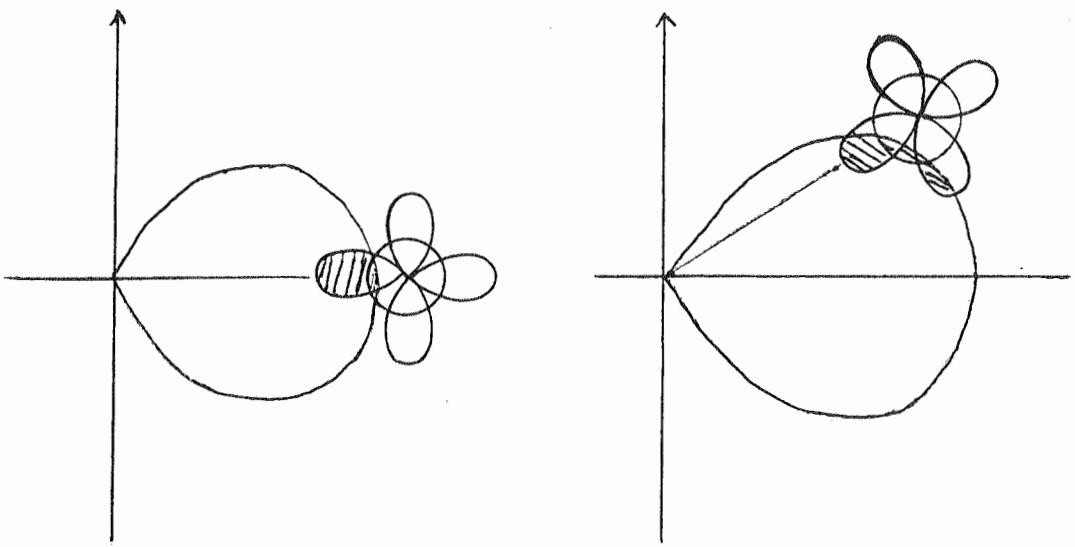

Figure 6.1 : variations in overlap between the groundstate and ligand 4s and 4p orbitals

6.3 Nature of the Groundstate

For an ion of D_{4h} symmetry, we have $g_z = g_{||}$ and $g_x = g_y = g_{\perp}$, and hence the metal part of the groundstate wavefunction is composed purely of the $d_{x^2-y^2}$ orbital[46]. However, for $(enH_2)_2Zn[Cu]Br_6$, the g values are significantly rhombic (i.e. $g_x \neq g_y$) and the symmetry of the guest $[CuBr_4]^{2-}$ ion may only be interpreted in terms of a C_{2v} point group. In this case, both the $d_{x^2-y^2}$ and d_{z^2} orbitals transform as the irreducible A1 representation.[47] The groundstate wavefunction is therefore a mixture of these obitals.

First order perturbation theory gives the equations for the shifts in g values from the free electron g value[48] :

$$\Delta g_x = \frac{-2\lambda k_x 2 (a - 3b)^2}{E_{yz}} \qquad (6.3a)$$

$$\Delta g_y = \frac{-2\lambda k_y 2 (a - 3b)^2}{E_{xz}} \qquad (6.3b)$$

$$\Delta g_z = \frac{-8\lambda k_z 2 a^2}{E_{xy}} \qquad (6.3c)$$

Here E is the energy of the d orbital indicated by the subscript, λ is the spin-orbit coupling constant, and k the orbital reduction parameter[49]. The wavefunction may be written as[48] :

$$\Psi = \frac{KR}{r^2} | cx^2 + ey^2 + fz^2 > \qquad (6.4)$$

where the wavefunction parameters c, e and f are related to the mixing coefficients a and b by [48] :

$$c = b + \sqrt{3}a \qquad (6.5a)$$

$$e = b - \sqrt{3}a \qquad (6.5b)$$

$$f = -2b \qquad (6.5c)$$

The ligand orbital overlap, which directly relates to the size of the groundstate lobes, is proportional to the magnitudes of c, e and f, while the squares of these parameters give the probability distribution along a specified axis[46]. Fitting the calculated g shifts to equations 6.3 and using the measured values of E_{xy}, E_{xz} and E_{yz} from chapter 3, gives a = 0.97 and b = 0.153. The corresponding values of c, e and f are shown in Table 6.3, with the groundstate shown schematically in Figure 6.2.

Table 6.3 Wavefunction parameters for $(enH_2)_2Zn[Cu]Br_6$

wavefunction parameters	probability along axes (%)	
c = 1.833	x	58.1
e = -1.527	y	40.3
f = -0.306	z	1.6

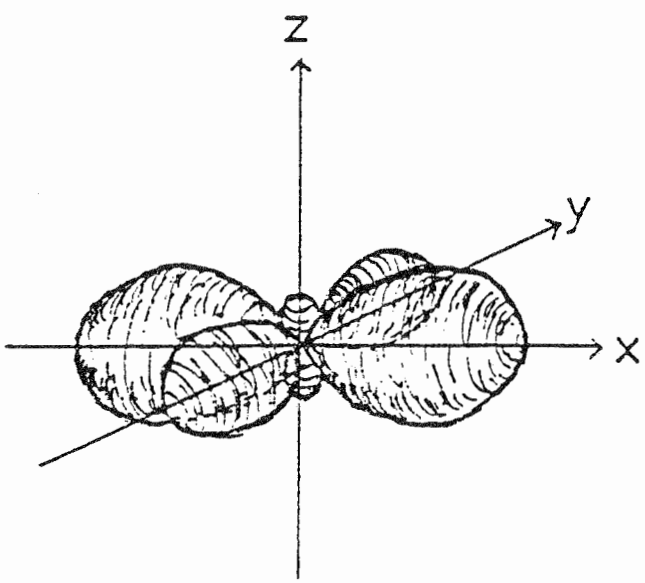

Figure 6.2 : shape of the groundstate wavefunction

It should be noted that the d-orbitals in a metal complex are anti-bonding, and for Cu^{2+}, the groundstate orbital is the only orbital half-filled with electrons.

As expected, the largest lobes correspond to the direction of the greatest ligand perturbation. However, there are also significant lobes along the z axis which, although having a relatively small occupancy, do deserve comment. For a pure $d_{x^2-y^2}$ orbital, equation (6.4) requires $c = e = \sqrt{3}$ and $f = 0$, while for $c = 2$ and $e = f = -1$, the groundstate wavefunction becomes d_{x^2} (more formally written as $d_{2x^2-z^2-y^2}$). Thus, inclusion of a d_{x^2} orbital in the groundstate creates a

wavefunction in which, relative to a pure $d_{x^2-y^2}$ orbital, the lobe along the molecular x axis is increased, the lobe along y is decreased and an extra lobe occurs along the z axis. From the experimentally determined value for f, it may be concluded that the groundstate is composed of approximately two - thirds $d_{x^2-y^2}$ and one - third d_{x^2}.

6.4 Analysis of the Hyperfine Parameters

It has long been known[2,43,50] that the observed hyperfine coupling constants for pseudotetrahedral copper (II) complexes cannot be successfully interpreted by means of equations 6.6 (a) - (c) as shown [48] :

$$A_x = P[\ -\kappa\alpha^2 + \frac{2\alpha^2(a^2 - b^2)}{7} + \frac{4\sqrt{3}\alpha^2 ab}{7} + \Delta g_x - \frac{(3a - \sqrt{3}b)\Delta g_y}{14\,(a + 3b)} - \frac{\Delta g_z b}{7a}\ ] \qquad (6.6a)$$

$$A_y = P[\ -\kappa\alpha^2 + \frac{2\alpha^2(a^2 - b^2)}{7} + \frac{4\sqrt{3}\alpha^2 ab}{7} + \Delta g_y - \frac{(3a + \sqrt{3}b)\Delta g_x}{14\,(a - 3b)} - \frac{\Delta g_z b}{7a}\ ] \qquad (6.6b)$$

$$A_z = P[\ -\kappa\alpha^2 - \frac{4\alpha^2(a^2 - b^2)}{7} + \frac{(3a - \sqrt{3}b)\Delta g_y}{14\,(a + 3b)} + \frac{(3a + \sqrt{3}b)\Delta g_x}{14\,(a - \sqrt{3}b)} + \Delta g_z\ ] \qquad (6.6c)$$

where a, b and $\Delta g_{x,y,z}$ are defined in the previous section. The parameter α^2 represents the fraction of time the unpaired electron spends in the metal d orbitals. The constant P[51] is taken to be 0.036 cm^{-1} for a copper (II) ion, while the Fermi contact parameter $\kappa = 0.43$ [52].

The nature of the E.S.R results have only permitted reliable values for

A_y and A_z, as the hyperfine splitting was not well resolved along the molecular x axis. However, it is possible to solve equations 6.6 (b) and (c). Using the literature values for P and κ together with the experimental values for A_y and A_z actually over-determines α, i.e there are two equations to verify *one* unknown. This procedure yields a value of $\alpha^2 \simeq 0.51$, compared with a value of 0.6 obtained from analysis of the superhyperfine coupling constants in section 6.3. Solving equations 6.6 (b) and (c) simultaneously, using $\alpha^2 = 0.6$, gives $P \simeq 0.01$ and $\kappa = 0.42$. Thus, to obtain a reasonable agreement, the free ion values of P and κ must be substantially reduced. Several explanations for these low values in pseudo-tetrahedral complexes have been proposed.

Yokoi[53] concluded that the distortion from a planar to a tetrahedral geometry was accompanied by a progressive decrease in κ. The dominant cause of this was rationalized in terms of a 3d - 4s spin polarisation mechanism. This could be applicable to the present work, as in C_{2v} symmetry, both the metal 4s and $3d_{z^2}$ orbitals transform as the same irreducible representatiom, and may therefore mix. For copper-doped NH_4Br, a low value of κ was also observed[54], and was accounted for by the mixing of approximately 3% of the 4s metal orbital into the predominantly $3d_{z^2}$ groundstate. The analogous situation may occur for $(enH_2)_2Zn[Cu]Br_6$, where the presence of the small lobes along the z axis permits a direct participation of the 4s orbital in the groundstate wavefunctions.

6.5 Discussion

Given that the ligands of the copper ion tend to move towards the lobes of the groundstate, the increase in α results in an increase of the groundstate lobe along x. This, in turn, favours a further increase in α. A synergic effect is therefore observed, where the nature of the distortion advocates further distortion. Moreover, a large value of α would be expected to contradict ligand-ligand repulsions. Thus, it may be argued that ligand-ligand repulsions act to decrease α,

while the synergic interaction acts in an opposite fashion, providing the geometrical balance.

From the spectral simulation studies discussed in chapter 5, self-consistent results were obtainable only when the z axis of the superhyperfine tensor was directed at an angle of ~43^{o} to the molecular z axis, rather than along the metal-ligand bond. For planar complexes, symmetry arguments constrain the superhyperfine z' axis to lie along the metal-ligand bonds. However, there is no reason why this should be the case for complexes of other symmetries. A possible explanation for the observed result is that the z' axis of the superhyperfine tensor bends away from the metal-ligand bond vector towards the lobe of the metal part of the groundstate.

CHAPTER 7
EPILOGUE

Throughout the report, various aspects of the structure and bonding in the $[CuBr_4]^{2-}$ ion have been discussed. Results have shown that successful application of E.S.R and Electronic spectroscopic techniques may provide an insight into the electronic and geometric structure of a doped ionic species, in an environment it may not normally occupy. The approach to the analysis of the data obtained, permits an extension of this work into the realm of structure identification of tetrahedrally coordinated copper in various metalloproteins.

As is the case for the majority of scientific research, this study has invoked more questions and experiments than it is possible to perform in the alloted time. Listed below is a compilation of suggestions for future work in this area.

1. measurement of Q band E.S.R spectrum for $(enH_2)_2Zn[Cu]Br_6$ at 77K, for a resolution of superhyperfine structure along the molecular x axis ;
2. subsequently, a more complete execution of the spectral simulations, to include A_X' and restrict the limits for θ ;
3. a full analysis of the charge transfer spectrum ;
4. consideration of bond length perturbations in the optimisation of the AOM parameters ;
5. extension to other host lattices and/or guest species .

This list is, of course, by no means complete.

REFERENCES

1. Hoffmann, S. K. and Goslar, J., *J. Solid State Chem.,* 1982, **44**, 343
2. Bencini, A., Gatteschi, D. and Zanchini, C., *J. Am. Chem. Soc.,* 1980, **102**, 5234
3. Jahn, H. A. and Teller, E., *Proc. Roy. Soc. London.,* 1937, **161**, 220
4. McDonald, R. G., Ph. D. Thesis, University of Tasmania, 1988
5. Cotton, F. A. and Wilkinson, G., " Advanced Inorganic Chemistry, 4^{th} ed. " (John Wiley and Sons : U.S.A. 1973.)
6. Sharnoff, M., Reimann, C., *J. Chem. Phys.,* 1965, **43**, 2993
7. Hathaway, B. J., *Coord. Chem. Rev.,* 1981, **35**, 211
8. Hitchman, M. A., Deeth, R. J., Lehmann, G. and Sachs, H., *Inorg. Chem.,* 1984, **23**, 1310
9. McDonald, R. G., Riley, M. J. and Hitchman, M. A., *Inorg. Chem.,* 1988, **27**, 894
10. Chow, C., Chang, K. and Willett, R. D., *J. Chem. Phys.,* 1973, **59**, 2629
11. De, D. K., *J. Chem. Phys.,* 1983, **79**(2), 535
12. Goodgame, M. L. and Leach, G. A., *J. Chem. Soc. Dalt. Trans.*, 1978, 1705
13. Colton. D. F. and Geary, W. J., *J. Inorg. Nucl. Chem.,* 1974, **36**, 1499
14. Osborne, R. R. and McWhinnie, W. R., *J. Chem. Soc (A).*, 1967, 2075
15. Deeth, R. J., Honours Thesis, University of Tasmania, 1981
16. Anderson, D. N. and Willett, R. D., *Inorg. Chem. Acta.,* 1971, **5**, 41
17. Morosin, B. and Lingafelter, E. C., *Acta. Cryst.,* 1959, **12**, 744; 1960, **13**, 807
18. Heming, M., Lehmann, G., Henkel, G. and Krebs B., *Zeutschrift feur Naturforschung.,* 1981, **36A**, 286
19. Trouelan, P., Lefebvre J. and Derollez, P., *Acta. Cryst.,* 1984, **C40**, 386; 1985, **C41**, 846

20. Day, P., *Angew. Chem. Int. Ed. Engl.*, 1980, **19**, 290

21. Hartshorne, N. H. and Stuart, A., " Crystals and the Polarising Microscope " (Edward Arnold : London. 1960)

22. Harlow, R. L., Wells, W. J., Watt, G. W. and Simonsen, S. H., *Inorg. Chem.*, 1975, **14**, 1768

23. Lever, A. B. P., " Inorganic Electronic Spectroscopy. " (Elsevier Science : Amsterdam. 1984)

24. Hathaway, B. J. and Billing, D. E., *Coord. Chem. Rev.*, 1970, **5**, 143

25. Desjardins, S. R., Penfield, K. W., Cohen, S. L., Musselman, R. L. and Solomon, E. I., *J. Am. Chem. Soc.*, 1983, **105**, 4590

26. Lehmann, G., *Chem. Phys. Lett.*, 1979, **65**, 184

27. Aramburu, J. A.,Moreno, M. and Bencini, A., *Chem. Phys. Lett.*, 1987, **140**, 462

28. Penfield, K. W., Gay, R. R., Himmelwright, R. S., Eickman, N. C., Norris, V. A., Freeman, H. C. and Solomon, E. I., *J. Am. Chem. Soc.*, 1981, **103**, 4382

29. Schåffer, C. E., *Structure and Bonding*, 1973, **14**, 69

30. Jørgensen, C. K., Pappalardo, R. and Schmidtke, H. H., *J. Chem. Phys.*, 1963, **39**, 1422

31. Schåffer, C. E. and Jørgensen, C. K., *J. Mol. Phys.*, 1965, **9**, 401

32. Schåffer, C. E., *Structure and Bonding*, 1968, **5**, 68

33. Larsen, E. and La Mar, G. N., *J. Chem. Ed.*, 1974, **51**, 633

34. Smith, D. W., *Structure and Bonding.*, 1972, **12**, 49

35. Bermejo, M. and Pueyo, L., *J. Chem. Phys.*, 1983, 78, 854

36. Cruse, D. A., Davies, J. E., Gerloch, M., Harding, J. H., Mackey, D. J. and McMeeking, R. F., " CAMMAG, A Fortran Computing Package. " University Chemical Laboratory : Cambridge, England

37. Cruse, D. A. and Gerloch, M, *J. Chem. Soc. Dalt. Trans.*, 1977, 1617

38. McDonald, R. G., Riley, M. J. and Hitchman, M. A., Inorg. Chem., 1988, **27**, 894

39. Wertz, J. E. and Bolton, J. R., " Electron Spin Resonance: Elementary Theory and Practical Applications. " (McGraw-Hill : U.S.A. 1972)

40. Artherton, N. M., " Electron Spin Resonance : Theory and Applications. " (John Wiley and Sons : U.S.A. 1973.)

41. Hitchman, M. A. and Belford, R. L., " Electron Spin Resonance of Metal Complexes "; Teh Fu Yen, Ed. (Plenum Press : New York. 1969)

42. Solomon, E. I. et. al., *Structure and Bonding*, 1983, **53**

43. Kokoszka, G. F., Reimann, C. W. and Allen, H. C., *J. Chem. Phys.*, 1967, **71**, 121

44. Morton, J. R. and Preston, K. F., *J. Mag. Res.*, 1978, **30**, 577

45. Stratemeier, H., Riley, M. J., Hitchman, M. A., Steffen, D. and Reinen, D., *Inorg. Chem.*, in press

46. Hitchman, M. A., *J. Chem. Soc*, 1970, **A**, 4

47. Cotton, F. A., " Chemical Applications of Group Theory " (Interscience : New York. 1963)

48. McGarvey, B. R., " Electron Spin Resonance of Transition Metal Complexes " Transition Metal Chemistry ed. (Marcel Dekker, Inc. : 1966)

49. Gerloch, M. and Miller, J. R., *Prog. Inorg. Chem.*, 1968, **10**, 1

50. Bertini, I., Canti, G., Grassi, R. and Scozyafava, A., *Inorg. Chem.*, 1980, **19**, 2198

51. McGarvey, B. R., *J. Phys. Chem.*, 1967, **71**, 51

52. Sharnoff, M., *J. Chem. Phys.*, 1965, **42** (4), 3383

53. Yokoi, H. and Addison, A. W., *Inorg. Chem.*, 1977, **16**, 1341

54. Narayana, P. A. and Sastry, K. L. V. N., *J. Chem. Phys.*, 1972, **57**, 3266

APPENDIX A

values of g^2 vs. η for the three rotations of $(enH_2)_2Zn[Cu]Br_6$

rotation 1 - ab plane

η	g^2	η	g^2	η	g^2	η	g^2
0	5.0229	60	4.3438	105	4.1465	150	4.8378
15	4.9057	75	4.2160	120	4.3940	165	4.9532
30	4.7930	90	4.2053	135	4.6599		
45	4.5347						

rotation 2 - ac plane

η	g^2	η	g^2	η	g^2	η	g^2
0	5.0872	60	5.3481	105	4.4935	150	4.6070
15	5.3259	75	5.0616	120	4.4049	165	4.8061
30	5.4522	90	4.7115	135	4.4024	180	5.1030
45	5.4639						

rotation 3 - bc plane

η	g^2	η	g^2	η	g^2	η	g^2
0	4.1922	60	4.5937	105	4.8131	150	4.4146
15	4.1767	75	4.7799	120	4.7484	165	4.2543
30	4.2572	90	4.8334	135	4.5211	180	5.1964
45	4.4269						

values of g^2 vs. η for the three rotations of $(enH_2)CuBr_4$

rotation 1 - ab plane

η	g^2	η	g^2	η	g^2	η	g^2
0	4.3802	60	4.2754	105	4.1939	150	4.2969
15	4.3819	75	4.2296	120	4.2111	165	4.3472
30	4.3731	90	4.1968	135	4.2465	180	4.3773
45	4.3227						

rotation 2 - ac plane

η	g^2	η	g^2	η	g^2	η	g^2
0	4.3631	60	4.2861	105	4.1914	150	4.2717
15	4.3773	75	4.2304	120	4.2046	165	4.3239
30	4.3631	90	4.2033	135	4.2304	180	4.3648
45	4.3334						

rotation 3 - bc plane

η	g^2	η	g^2	η	g^2	η	g^2
0	4.3798	60	4.3714	105	4.3882	150	4.3924
15	4.3769	75	4.3744	120	4.3936	165	4.3839
30	4.3648	90	4.3811	135	4.3962	180	4.3811
45	4.3677						

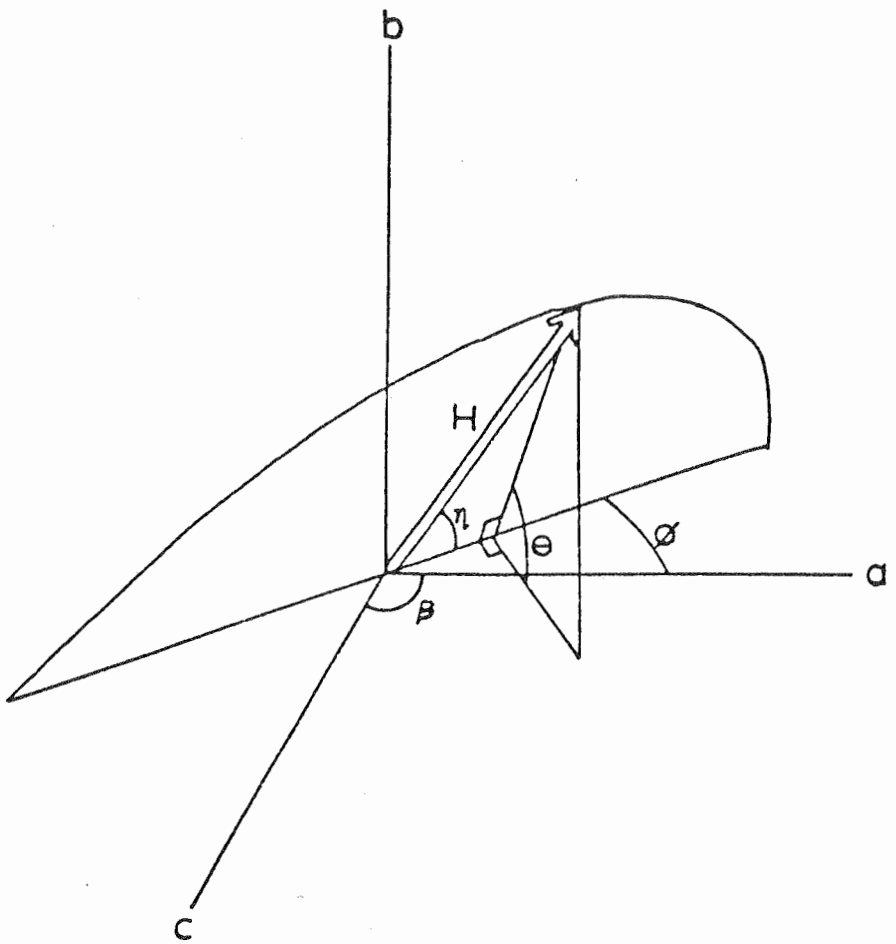

Figure A.1 : angles defining the magnetic vector **H** in terms of a monoclinic crystal coordinate system

note :- for monoclinic systems, $\beta^* \neq 90^o$

APPENDIX B.
COMPUTER PROGRAMS

B.1 Introduction

Throughout this project, a significant proportion of the time was devoted to the modification and use of computer programs as an aid in analysing the data. All programs were written in FORTRAN and operated on the University of Tasmania PRIMEB Network. It is beyond the scope of this work to explain, in detail, the mathematical operations behind the programs. However, their use does justify some discussion.

B.2 ' GTENSOR '

As mentioned in chapter 3, calculation of the principal g values was accomplished with the use of the ' GTENSOR ' program. This program was used without modification. General operation proceeds with the supply of an input file containing the following data :

- space group of the molecule
- definition of the molecular x axis
- slow or fast electron exchange
- fractional coordinates of the atoms
- unit cell lengths (a,b,c) and angles (α,β,γ)
- number of rotation planes and measurements in each plane
- angles for the orientation of the magnetic field (η)
- measured g values from experimental E.S.R spectra

The resulting output may then be considered in four separate portions.

Firstly, for geometrical purposes, the metal-ligand bond lengths in the $[CuBr_4]^{2-}$ ion are calculated, along with all possible bond angles [Figure B.1]. Secondly, for each rotation, a table is presented, which displays the crystal and

molecular coordinates, and the measured and calculated g values for each experimental value of η [Figure B.2]. The third segment of the output presents the results in a similar fashion as previously explained. In this case, however, a refinement is made which optimizes the orientation of the molecular planes within the magnetic field (i.e the values of η) so that equivalent positions in the magnetic field give coincident g values [Figure B.3]. Finally the matrix for the **g** tensor is then calculated, and diagonalised with respect to the molecular coordinate system. This gives the principal **g** values along each axis, and the euler angles which relate the axes of the **g** tensor to the molecular axis system [Figure B.4].

B.3 ' SIMGEN '

SIMGEN is a simulation program that calculates the lineshapes for single crystal E.S.R spectra. In this case, a program written by Dr. Horst Stratemeier was modified for the present problem. Various parameters are permanently stored in a data file, these being

- the number of ligands
- the ligand spin
- the metal ion spin
- the isotope ratio
- the magnetic moment ratio

The remaining parameters needed for complete execution of the program were

- the magnetic field limits
- principal g values
- hyperfine tensor values
- superhyperfine tensor values

These were all necessarily adjusted for each simulation.

In order to relate the magnetic field to the superhyperfine tensor, it is easiest to employ a universal coordinate system. The magnetic field is usually defined in respect to the molecular system, which, for previous versions of this

UNIT CELL DIMENSIONS:

A:	6.719	B:	19.923	C:	6.434
ALPHA:	90.000	BETA:	93.210	GAMMA:	90.000

BOND LENGTHS IN ANGSTROM:

ZN	- BR1	:	1.1379
ZN	- BR2	:	2.3964
ZN	- BR3	:	2.4099
ZN	- BR4	:	2.4558
ZN	- BR0	:	2.3964
ZN	-	:	8.0873

BOND ANGLES IN DEGREES :

BR1 - ZN	BR2 - ZN	BR3 - ZN	BR4 - ZN	BR0 - ZN	- ZN
0.00	61.65	131.62	120.72	61.65	43.90
61.65	0.00	108.39	104.04	123.30	27.85
131.62	108.39	0.04	107.66	108.39	135.79
120.72	104.04	107.66	0.00	104.04	95.41
61.65	123.30	108.39	104.04	0.00	101.53
43.90	27.85	135.79	95.41	101.53	0.00

ATOMIC COORDINATES

	X/A	Y/B	Z/C
ZN	0.91353	0.25000	0.32441
BR1	0.78307	0.25000	0.20375
BR2	0.78307	0.14414	0.20375
BR3	1.26868	0.25000	0.28884
BR4	0.85623	0.25000	0.69805
BR0	0.78307	0.35586	0.20375
	0.00000	0.00000	0.00000

Figure B.1 : crystallographic data for $(enH_2)_2Zn[Cu]Br_6$

ROTATION: 1

NUMBER OF MEASUREMENTS: 12

THETA: 90.0 PHI: 0.0 AVERAGE RESIDUAL: 0.03455 REFINEMENT ADJUSTMENT: 0.0000 DEGREES

NU	CRYSTAL COORDINATES A	B	C	MOLECULAR COORDINATES x*x	y*y	z*z	AVERAGE TENSOR COORDS i	j	K	MEASURED g	CALCULATED g	DIFFERENCE Delta g
0.00	0.0000	0.0000	1.0000	0.3012	0.1073	0.5915	0.5875	0.1958	0.7852	2.24120	2.24791	-0.00671
15.00	0.0000	0.2588	0.9659	0.4392	0.0089	0.5519	0.4829	0.4337	0.7607	2.21490	2.2	0.01519
30.00	0.0000	0.5000	0.8660	0.5351	0.0212	0.4437	0.3454	0.6421	0.6844	2.18930	2.19028	-0.00098
45.00	0.0000	0.7071	0.7071	0.5631	0.1411	0.2958	0.1843	0.8067	0.5615	2.12950	2.13831	0.00881
60.00	0.0000	0.8660	0.5000	0.5158	0.3363	0.1479	0.0107	0.9163	0.4003	2.08420	2.08774	-0.00354
75.00	0.0000	0.9659	0.2588	0.4058	0.5546	0.0396	0.1636	0.9635	0.2118	2.05330	2.05268	0.00062
90.00	0.0000	1.0000	0.0000	0.2626	0.7374	0.0000	0.3268	0.9450	0.0089	2.05070	2.04347	0.00724
105.00	0.0000	0.9659	-0.2588	0.1246	0.8358	0.0396	0.4677	0.8622	0.1946	2.06360	2.06290	0.00070
120.00	0.0000	0.8660	-0.5000	0.0287	0.8234	0.1479	0.5768	0.7205	0.3849	2.09620	2.10512	-0.00892
135.00	0.0000	0.7071	-0.7071	0.0007	0.7036	0.2958	0.6465	0.5298	0.5489	2.15870	2.15789	0.00081
150.00	0.0000	0.5000	-0.8660	0.0480	0.5083	0.4437	0.6722	0.3030	0.6755	2.19950	2.20685	-0.00735
165.00	0.0000	0.2588	-0.9659	0.1580	0.2901	0.5519	0.6521	0.0555	0.7561	2.22560	2.23950	-0.01390

Figure B.2 : calculated and measured g values for $(enH_2)_2Zn[Cu]Br_6$

ROTATION: 3

NUMBER OF MEASUREMENTS: 12

THETA: 90.0 PHI: 0.0 AVERAGE RESIDUAL: 0.02009 REFINEMENT ADJUSTMENT: 2.9522 DEGREES

NU	CRYSTAL COORDINATES A	B	C	MOLECULAR COORDINATES x*x	y*y	z*z	AVERAGE TENSOR COORDS i	j	K	MEASURED g	CALCULATED g	DIFFERENCE Delta g
2.95	0.0000	0.0515	0.9987	0.3300	0.0800	0.5900	0.6416	0.0952	0.7611	2.24120	2.23892	0.00228
17.95	0.0000	0.3082	0.9513	0.4625	0.0022	0.5353	0.5902	0.3490	0.7279	2.21490	2.22155	-0.00665
32.95	0.0000	0.5439	0.8391	0.5465	0.0370	0.4165	0.4987	0.5790	0.6450	2.18930	2.18321	0.00609
47.95	0.0000	0.7426	0.6698	0.5596	0.1750	0.2653	0.3731	0.7696	0.5182	2.12950	2.13341	-0.00391
62.95	0.0000	0.8906	0.4547	0.4984	0.3793	0.1223	0.2221	0.9077	0.3561	2.08420	2.08517	-0.00097
77.95	0.0000	0.9780	0.2087	0.3791	0.5951	0.0258	0.0560	0.9839	0.1697	2.05330	2.05194	0.00136
92.95	0.0000	0.9987	-0.0515	0.2338	0.7647	0.0016	0.1139	0.9931	0.0282	2.05070	2.04349	0.00721
107.95	0.0000	0.9513	-0.3082	0.1013	0.8425	0.0562	0.2761	0.9346	0.2243	2.06360	2.06236	0.00124
122.95	0.0000	0.8391	-0.5439	0.0173	0.8077	0.1750	0.4194	0.8124	0.4050	2.09620	2.10290	-0.00670
137.95	0.0000	0.6697	-0.7426	0.0041	0.6697	0.3262	0.5342	0.6349	0.5582	2.15870	2.15341	0.00529
152.95	0.0000	0.4547	-0.8906	0.0654	0.4654	0.4692	0.6126	0.4141	0.6733	2.19950	2.20015	-0.00065
167.95	0.0000	0.2087	-0.9780	0.1847	0.2495	0.5658	0.6492	0.1650	0.7425	2.22560	2.23118	-0.00558

Figure B.3 : table from B.2 with refinement for orientation

EIGENVALUES	EIGENVECTORS IN MOLECULAR COORDS			EULER ANGLES
	x	y	z	DEGREES
2.0915	-0.81450	0.58003	0.01251	50.7
2.0426	0.58015	0.81445	0.01001	179.1
2.3408	-0.00438	0.01541	-0.99987	-167.1
2.0915	-0.89722	0.44141	0.01251	50.7
2.0426	-0.44131	-0.89730	0.01001	0.9
2.3408	0.01564	0.00346	0.99987	102.7

Figure B.4 : principal g values and direction cosines for **g** tensor

program, implied that the ligand should lie along the molecular axes. This is, of course, impossible for an ion of tetrahedral (or even pseudotetrahedral) symmetry. The SIMGEN program overcomes this problem by calculating the projection of the superhyperfine tensor onto each molecular axis. Hence, the position of each ligand was specified uniquely by defining the angles between each of the corresponding superhyperfine tensor axes and each molecular axis.

B.4 'CAMMAG'

This program was originally developed by Gerloch and colleagues[36], and, in this work, is used to calculate a set of theoretical d-d transition energies, based on the Angular Overlap Model. Operation requires the use of two segments designated SETUP and RUN.

Input data for the SETUP section comprises a description of the molecular geometry with respect to the metal ion. In addition, a local cartesian frame for the ligands is defined in terms of the various metal-ligand bond vectors.

The main body of the RUN section comprises the values of e_σ and e_π for each ligand in the system. Other neccessary data includes

- a definition of the crystal system
- spin-orbit coupling constant for the Cu^{2+} ion
- orbital reduction parameter

Racah parameters, expressed in CAMMAG as Condon-Shortley electron repulsion parameters, are normally required. However, for a d^9 system, the basis function may be described by the ^2D term only. Thus the absence of higher energy terms dispenses the need for such parameters in this work.

The ouput from the SETUP file presents a review of the molecular and the ligand coordinate systems, as defined from the input. However, its primary function is to create the necessary data files for use in subsequent calculations.

From the output of the RUN file, the most appropriate segment for this work is shown in Figure B.5. Here, the theoretical energies for the d-d transitions are calculated from the values stored in the data files mentioned above.

EIGENVALUES

			PROJECTIONS OF REPRESENTATIONS				
			A1	B1	B2	B3	(D2)
LEVEL	ENERGY	RELATIVE ENERGY	A1	A2	B1	B2	(C2V)
10	2993.09	8303.02	0.11	0.03	0.80	0.06	
9	2993.09	8303.02	0.11	0.03	0.80	0.06	
8	2662.03	7971.96	0.02	0.46	0.04	0.49	
7	2662.03	7971.96	0.02	0.46	0.04	0.49	
6	819.46	6129.39	0.01	0.51	0.04	0.44	
5	819.46	6129.39	0.01	0.51	0.04	0.44	
4	-1164.66	4145.27	0.97	0.01	0.01	0.01	
3	-1164.66	4145.27	0.97	0.01	0.01	0.01	
2	-5309.93	0.00	0.89	0.00	0.10	0.00	
1	-5309.93	0.00	0.89	0.00	0.10	0.00	

Figure B.5 : calculated d-d transition energies